

The Assessment of Morphologic Bilateral Asymmetry in Knees with and without Trochlear Dysplasia

by

Julia van den Heiligenberg

A master's thesis

Submitted to the Faculty of Science and Technology

University of Twente

In partial fulfilment of the requirements
for the degree of Master of Science

in

Technical Medicine

Track Medical Imaging & Interventions

June 25th, 2024

Graduation Committee

Chairman & Technological Supervisor

Prof. dr. ir. N.J.J. Verdonschot

Faculty of Engineering Technology (ET), Biomedical Device Design and Production
Technology (BDDP) / Department of Orthopaedic Surgery

University of Twente / Radboudumc

Medical Supervisor

Dr. ing. S.A.W van de Groes

Department of Orthopaedic Surgery

Radboudumc

Technical Medicine Supervisor

Drs. E.H.S. Teule

Department of Orthopaedic Surgery

Radboudumc

Process Supervisor

Drs. N.S. Cramer Bornemann

Faculty of Science and Technology (TNW)

University of Twente

External Member

Dr. ir. F.F.J. Simonis

Faculty of Science and Technology (TNW), Magnetic Detection and Imaging (MD&I)

University of Twente

Voorwoord

Deze scriptie vormt het laatste inhoudelijke deel in de afronding van mijn studie Technische Geneeskunde. De afronding van de master Medical Imaging & Interventions heeft plaatsgevonden tijdens mijn afstudeerstage bij de afdeling Orthopedie in het Radboudumc, waar ik een jaar lang welkom en uitgedaagd ben geweest om mijzelf te ontwikkelen tot volwaardig technisch geneeskundige.

Het is op zijn plaats om de mensen te bedanken die ervoor hebben gezorgd dat ik niet alleen inhoudelijk ben uitgedaagd om mij op klinisch, technologisch en wetenschappelijk niveau te ontwikkelen, maar ook op professioneel en persoonlijk vlak. Ik heb tijdens dit afstudeerjaar immers alle ruimte gekregen om te groeien tot de technisch geneeskundige die ik graag wilde worden.

Ten eerste wil ik Miriam bedanken, omdat ik op elk moment bij haar terecht kon met vragen en tijd maakte voor mij. Miriam heeft altijd meegedacht over de denkstappen in het onderzoek en hielp actief hierbij mee. Ze vulde mij aan tijdens meetings op momenten dat ik het nodig had. Daarnaast heeft ze altijd gevraagd hoe het met mij ging en gaf ze met haar feedback mij een goed gevoel. Dat waardeer ik zeer. Dat zij niet in de lijst met commissieleden mag staan, zie ik als een domper op het afstudeerjaar.

Ik wil daarvoor Erin bedanken, omdat zij deze plek als technisch geneeskundige heeft willen opvullen en veel heeft bijgedragen aan denkprocessen en veel kwalitatieve feedback in deze stage. Samen met Miriam heeft Erin mij ondersteund vanuit een wetenschappelijk technisch-medisch perspectief, en heeft zij mij op mijn gemak laten voelen op de afdeling. Daarbij vond ik de verhalen en foto's van de verbouwing van haar bus altijd heel leuk en inspirerend.

Daarnaast wil ik Nico bedanken. Bij het eerste gesprek met hem heeft hij mij aangegeven dat mijn stage prioriteit was en mijn welzijn hoog in het vaandel staat. Zo heb ik dat tijdens dit jaar zeker gevoeld en hij heeft mij hier altijd aan herinnerd. Daarbij waren onze meetings waardevolle sessies voor de wetenschappelijke waarde van deze scriptie en heb ik hierdoor veel mogen leren.

Ook bedank ik Sebastiaan, voor de uitdaging om een assertievere houding aan te nemen in de kliniek, waardoor ik met meer zelfvertrouwen de rol van zorgverlener op mij kan nemen. Daarnaast heet hij mij na te laten denken over wat ik wil in mijn loopbaan, wat ik fijn vond. Ook waardeer ik zijn droge humor waardoor contact altijd leuk was.

Voor de afgelopen twee jaar wil ik Nicole bedanken. Door haar heb ik tijdens al mijn stages de herinnering gekregen dat het 'leren, experimenteren en genieten' prioriteit was boven het 'moeten en presteren'. Hierdoor heb ik dit door mijn stages heen meer kunnen doen, en hebben we samen met veel enthousiasme kunnen ervaren dat bij mij een doorbraak kwam in het genieten van mijn stages en het mogen laten zien van mijzelf.

Ook wil ik Frank bedanken, voor het aansluiten bij mijn commissie als buitenlid. Ik vind het fijn dat hij tijd vrijmaakt en geïnteresseerd is in mijn afstuderen, en hierbij de wetenschappelijke, inhoudelijke kwaliteit controleert.

Als laatste bedankt ik de lezer van deze scriptie, voor de interesse in mij en mijn afstudeeronderzoek. Veel leesplezier toegewenst!

Abstract

Introduction: Patellofemoral instability (PFI) is characterised by the dislocation of the patella from its normal anatomical position within the trochlear groove. Trochlear dysplasia significantly contributes to the onset of PFI by impairing the trochlea's ability to adequately support the patella, thereby increasing the risk of dislocation. Despite its clinical relevance, precise correction methods for trochlear dysplasia remain uncertain.

Background: For correction methods in orthopaedic surgery, the contralateral bone is often used as a reference, though a detailed morphological 3D analysis regarding knee symmetry has not been conducted. Because of this, it is not clear whether the contralateral side can be used in a trochlear correction whether trochlear dysplasia potentially produces more bilateral asymmetry. This study aims to elucidate the degree of morphological bilateral symmetry in the 3D anatomy of the knee, for knees with and without trochlear dysplasia, providing foundational insights for future research across various medical fields.

Method: We investigated whether the morphological bilateral symmetry of the knee bones (femur, patella, and tibia) varies between different regions of the bones, and between healthy subjects and patients with trochlear dysplasia. A mean bone was made of each of those three bones and was used as a template to calculate the surface distances between the left and right bones.

Results: In healthy subjects, the median degree of asymmetry was 1.3 ± 0.7 mm for the femur, 0.9 ± 0.2 mm for the patella and 1.4 ± 0.8 mm for the tibia. The degree of asymmetry was higher for the dysplasia knees, especially for the femur and patella. The medial condyle of the femur, the medial part of the patella and the lateral part of the tibial metaphysis were the regions with the most morphological bilateral asymmetry.

Conclusion: Therefore, it can be concluded that the bones of the knees are not morphological bilateral symmetrical and that the degree of asymmetry rises with the degree of trochlear dysplasia.

Table of Contents

- Graduation Committee..... ii
- Voorwoord..... iii
- Abstract..... iv
- List of figures vii
- List of tables vii
- List of abbreviations viii
- 1. Introduction to this Thesis 1
- 2. Clinical Background..... 2
 - 2.1 Anatomy and Physiology of the Knee 2
 - 2.1.1 Bones..... 2
 - 2.1.2 Muscles 3
 - 2.1.3 Ligaments..... 3
 - 2.1.4 Innervation..... 4
 - 2.2 Patellofemoral Instability..... 5
 - 2.2.1 Diagnostics 6
 - 2.2.2 Treatment 8
- 3. Technical Background 10
 - 3.1 Radiography and (4D) Computed Tomography 10
 - 3.2 Image Processing 11
 - 3.3 Statistical Shape Modelling..... 11
- 4. Introduction to this Research 13
- 5. Research Objectives..... 14
- 6. Materials & Methods 15
 - 6.1 Participants 15
 - 6.2 Data Collection..... 15
 - 6.3 Pre-processing of CT Scans 18
 - 6.4 Categorisation..... 20
 - 6.5 Healthy Mean Model 21
 - 6.6 Creating Regions 21
 - 6.7 Calculate Bilateral Asymmetry..... 23
- 7. Results 26
 - 7.1 Sub-goal 1..... 26
 - 7.1.1 Visualisations 26
 - 7.1.2 Quantification 31

7.1.3 Statistics	31
7.2 Sub-goal 2.....	33
7.2.1 Visualisations	33
7.2.2 Quantification	37
7.2.3 Statistics	37
8. Discussion.....	41
8.1 Comparison with previous research	41
8.2 Strengths.....	41
8.3 Limitations.....	42
9. Clinical Relevance & Future Perspective.....	45
10. Conclusion.....	47
11. References	48
Appendix	51
A. MATLAB Codes.....	51
A1. Creating the Bone Meshes.....	51
A2. Mirror the Bone Meshes.....	52
A3. Cut the Bone Meshes.....	52
A4. CPD Registration	53
A5. Calculate Distances and Create the Colour maps.....	54
A6. Create an Artificial Radiography	55
B. ShapeWorks Settings	56

List of figures

1. The knee bones.	p. 2
2. Anterior view of the quadriceps muscles.	p. 3
3. Ligaments attached to the patella.	p. 4
4. Visualisation of patellofemoral instability.	p. 5
5. Characteristics of the four Dejour classification categories.	p. 7
6. Method to calculate the Caton-Deschamps index in a lateral radiograph.	p. 8
7. The influence of transmission angle on a knee X-ray.	p. 10
8. Pipeline with the method sections.	p. 15
9. Total of in-and exclusions of CT scans.	p. 17
10. A pipeline which shows the steps of converting a CT scan into meshes.	p. 18
11. Mirroring the left bone mesh.	p. 19
12. Cutting the bone mesh.	p. 20
13. Mean bone models.	p. 21
14. Regions of the bones.	p. 22
15. Exclusion of vertices of the femur and tibia.	p. 22
16. The function of the mean bone as template.	p. 24
17. A representation of the calculation of surface distances	p. 27
18. Histograms of the data of group 0.	p. 28
19. Colour maps of the femur, patella and tibia for group 0.	p. 30
20. Colour maps of the femur, patella and tibia per group.	p. 34
21. Segmentation error with bone fragment.	p. 43
22. Segmentation error with bipartite patella.	p. 43

List of tables

1. Median and IQR for the bones and for the regions in group 0.	p. 31
2. Results of the mixed models of the regions in the bones in group 0.	p. 32
3. Median and IQR for the bones and for the regions in all groups.	p. 37
4. Results of the mixed models of the bones in all groups.	p. 38
5. Results of the mixed models of the regions in the bones in all groups.	p. 39
6. ShapeWorks 'Optimize' Settings.	p. 56

List of abbreviations

- 2D – Two-Dimensional
- 3D – Three-Dimensional
- 4DCT – Four-Dimensional Computed Tomography
- CDI – Caton-Deschamps Index
- CPD – Coherent Point Drift
- CT – Computed Tomography
- ERC – European Research Community
- IQR – Interquartile Range
- MPFL – Medial Patellofemoral Ligament
- PFI – Patellofemoral Instability
- PFP – Patellofemoral Pain
- ROI – Region Of Interest
- SSM – Statistical Shape Model
- VOI – Volume Of Interest

1. Introduction to this Thesis

This thesis was written as a technical medicine graduation assignment on behalf of the University of Twente at the orthopaedics department of the Radboudumc. The research carried out during the graduation period revolves around determining the degree of morphological bilateral symmetry of knees with and without trochlear dysplasia. This assignment centres on a line of research that focuses on improving the treatment of patients with patellofemoral instability (PFI) through innovation in technology. To provide clinical and technological context, **Chapter 2 and 3** provide relevant background information. **Chapter 4 and 5** contain the introduction to the research and the objectives that will be achieved by conducting the study. The method section is outlined in **Chapter 6**, after which the results are presented in **Chapter 7**. **Chapters 8-10** set out the discussion, clinical relevance, future perspectives and conclusion of the study.

2. Clinical Background

The following paragraphs briefly describe the anatomy, physiology and pathology of the knee. Additionally, the diagnostic methods and therapies are described to provide information about the clinical context of PFI. This clinical background information can contribute to understanding the clinical reasoning and relevance of this thesis.

2.1 Anatomy and Physiology of the Knee

2.1.1 Bones

The knee consists of three major bones: the femur, the tibia, and the patella (1). Those bones form two joints: the tibiofemoral and patellofemoral joint. The bones of the knee are depicted in Figure 1 (2). The first bone of the knee is the femur. The distal epiphysis of the knee includes the medial and lateral condyles, which are large, rounded structures that articulate with the tibia and form the main parts of the knee joint. In between those condyles anteriorly, a U-shaped groove is formed: the trochlear groove. This groove runs in an anterior-posterior direction and interacts with the patella in the patellofemoral joint. The patella is the second bone of the knee and is a triangular shaped bone, anterior to the epiphysis of the femur. The apex of the triangular shape is oriented to caudal. The third bone of the knee is the tibia, which is a part of the tibiofemoral joint. The proximal epiphysis of the tibia consists of a tibial plateau, which forms the top surface of this bone. Anterior, more distal to the tibial plateau is the tibial tuberosity, which is a more prominent part of the bone and is connected to the patella by the patellar ligament (1). The intraarticular parts of the bones are covered with cartilage to facilitate smooth movement (1, 3). Thereby, a lateral and medial meniscus in between the femur and tibia provide pressure distribution over the tibiofemoral joint.

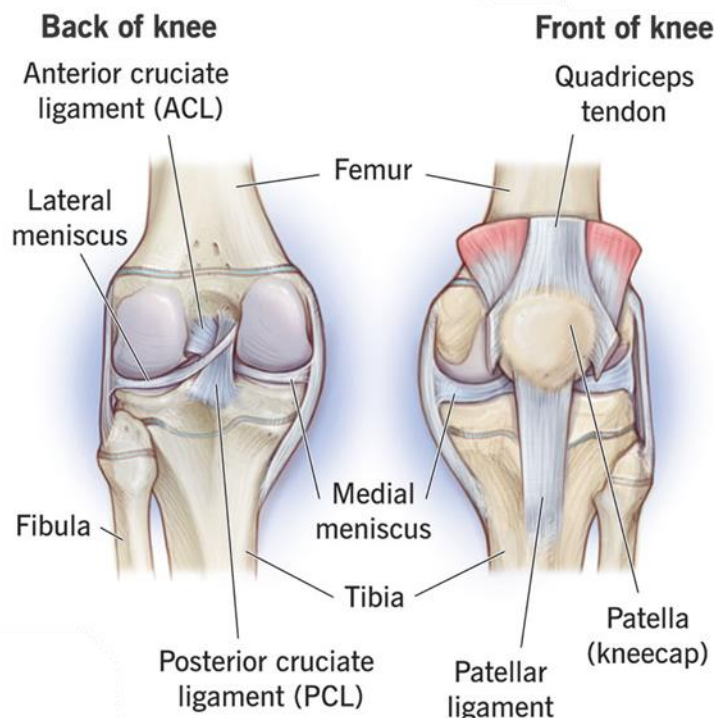


Figure 1: Bones of the knee (2).

2.1.2 Muscles

The muscles connected to the patellofemoral joint play a vital role in its function and stability. The primary muscles involved include the vastus lateralis, vastus medialis, vastus intermedius, and rectus femoris (Figure 2) (1, 4). These extend from the hip and thigh region and converge into the quadriceps tendon, which attaches to the patella at its proximal side.

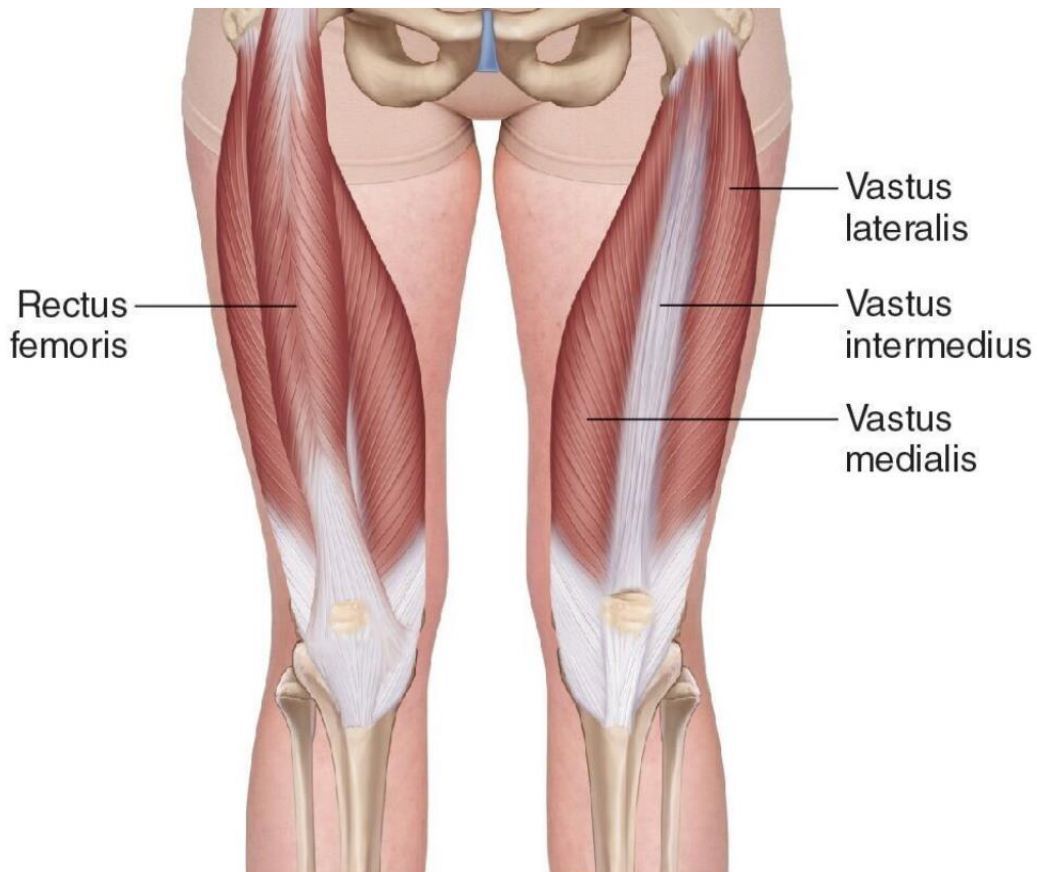


Figure 2: Anterior view of the quadriceps muscles (5)

2.1.3 Ligaments

The two knee joints allow movement in six directions: translation in three directions and rotation in three directions. Due to this complexity, it is crucial to stabilise the knee joint (6). This stabilisation is provided by four primary ligaments that provide stability to the tibiofemoral joint:

- Anterior Cruciate Ligament (ACL)
 - *Prevents:* excessive forward movement of the tibia relative to the femur.
 - *Stabilises:* rotational movements and hyperextension.
- Posterior Cruciate Ligament (PCL)
 - *Prevents:* excessive backward movement of the tibia relative to the femur.
 - *Stabilises:* activities like jumping and landing.
- Medial Collateral Ligament (MCL)

- *Prevents:* excessive medial movement of the tibia relative to the femur.
- *Stabilises:* valgus stress.
- Lateral Collateral Ligament (LCL)
 - *Prevents:* excessive lateral movement of the tibia relative to the femur.
 - *Stabilises:* varus stress.

The ligaments which stabilise the patellofemoral joint are (1, 7):

- Medial patellofemoral ligament (MPFL)
 - *Prevents:* excessive lateral movement of the patella relative to the femur.
 - *Stabilises:* patellar tracking.
- Lateral patellofemoral ligament (LPFL).
 - *Prevents:* excessive medial movement of the patella relative to the femur.
 - *Stabilises:* patellar tracking.
- Medial patellotibial ligament (MPTL).
 - *Prevents:* excessive lateral movement of the patella relative to the tibia.
 - *Stabilises:* patellar tracking.
- Lateral patellotibial ligament (LPTL).
 - *Prevents:* excessive medial movement of the patella relative to the tibia.
 - *Stabilises:* patellar tracking.

All four ligaments (Figure 3), particularly the MPFL, play a vital role in preventing lateral patellar dislocation and ensuring stability in patellar tracking and alignment during knee movement. The lack of stability from one or more of these ligaments could contribute to improper patellar tracking or patellar dislocation.

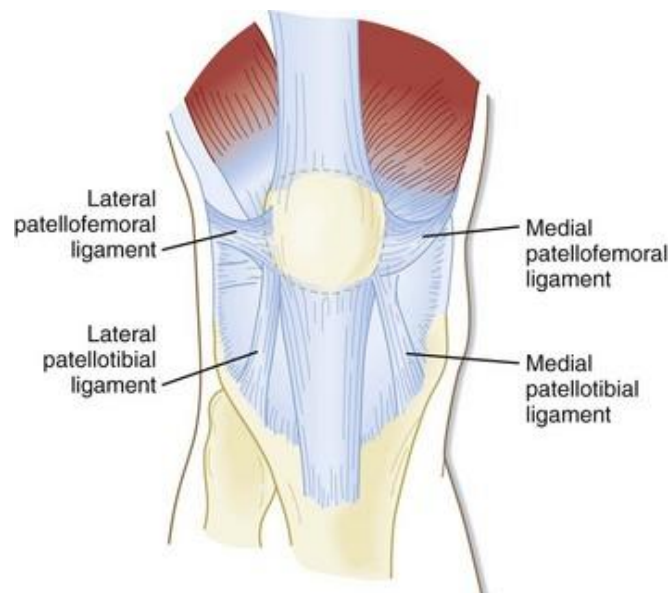


Figure 3: Ligaments attached to the patella (8).

2.1.4 Innervation

The innervation of the patellofemoral joint differs from that of the tibiofemoral joint. For the tibiofemoral joint articular branches of femoral, obturator, common fibular, tibial, and saphenous nerves constitute the nerve supply (9). For the patellofemoral joint, the main nerve responsible for

innervation is the femoral nerve (1). This nerve provides sensory innervation to the anterior aspect of the knee joint, including the patellar surface of the femur and the posterior surface of the patella. Additionally, branches of the obturator nerve also contribute to the innervation of the patellofemoral joint, particularly the parts of the joint located more medially.

2.2 Patellofemoral Instability

PFI occurs when the alignment between the patella and the trochlear groove of the femur is disrupted (Figure 4) (7, 10). This misalignment often leads to lateral displacement of the patella and predominantly affects individuals aged ten to twenty, with an annual incidence of 31 out of 100,000 within this age group (11). After the initial occurrence, recurrence of patellar luxations is common, affecting about 17% of all patients suffering from PFI (10).

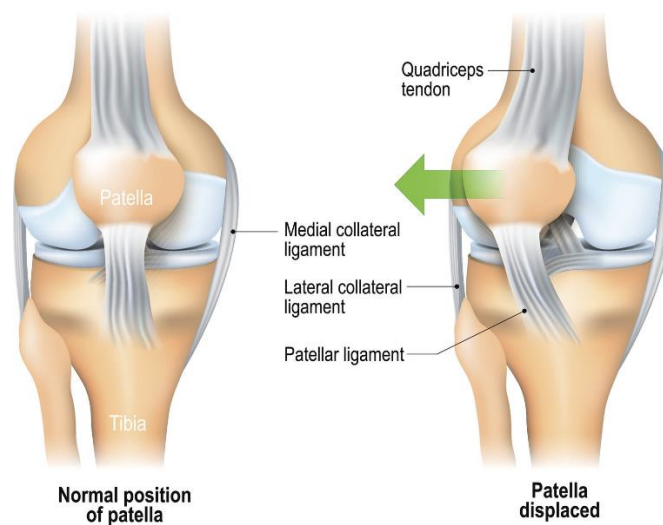


Figure 4: Visualisation of patellofemoral instability (12).

Patellar luxations typically manifest during sports activities and are frequently triggered by improper movements, such as external rotation of the lower leg coupled with slight knee flexion and inward stress on the knee joint (7, 10). While patellar luxations may spontaneously resolve upon knee extension, manual reduction may be required if spontaneous resolution does not occur.

Most people have the potential to experience a patellar luxation. However, certain individuals may be more predisposed to this due to the following contributing factors (7, 10):

- Trochlear dysplasia: morphological deformity of the femoral trochlea (shallow, flattened or convex), which can affect patellar tracking.
- Laxity of the MPFL: looseness of the MPFL, reducing medial traction on the patella.
- Patella alta: an abnormally high, proximal position of the patella, which delays the patella its entry in the trochlear groove during knee flexion.
- Knee valgus (the distal part of the lower leg is angled laterally): provides a more lateral position of the patella, which increases the risk of a lateral dislocation of the patella.
- Femoral anteversion (femoral neck is tilted forwards): alters the orientation of the trochlear groove and increases lateral tension on the patella.

- Conditions associated with hyperlaxity: reduces the patellofemoral stability provided by the knee ligaments.

These factors deteriorate the engagement of the patella with the trochlear groove, and this increases the risk of luxation.

PFI significantly impacts patients, manifesting as persistent symptoms like pain, discomfort, and a sense of knee insecurity. Activities requiring knee movement, including walking, running, or engaging in sports, may be limited or fully compromised. Furthermore, repeated episodes of patellar luxation can result in joint damage (specially the ligaments and cartilage), potentially necessitating surgical intervention to restore stability and alleviate symptoms (7, 10).

2.2.1 Diagnostics

The diagnosis of PFI typically relies on the anamnesis. During the anamnesis, the physician asks about the frequency and duration of patellar dislocations and any precipitating factors or specific activities that exacerbate symptoms. Also, the medical history of the patient is considered, including previous knee injuries or surgeries and any family history of knee problems or patellar instability. These questions are crucial for understanding the patient's condition, identifying potential contributing factors, and assessing the overall impact of PFI on their daily activities and quality of life.

In addition to the anamnesis, physical examination can be executed to investigate which treatment could be effective for the patient. This starts with inspection of the presentation and alignment of both knees. The temperature and swelling can be identified during palpation, increased temperature and swelling can indicate inflammation of the joint. Functionally, an increased patellar mobility or apprehension upon lateral displacement of the patella is assessed by the apprehension test. With this test, pressure is applied medially to patella while the knee is in extension. When no or little medial traction can be felt, there may be an indication of MPFL laxity. When the patient expresses apprehension to dislocation of the patella, there is an indication of a previous patellar dislocation. To assess patellar tracking, a positive J-sign can be verified. The J-sign is a sign in the patellar tracking, where the patella moves lateral in knee extension and forms the shape of a 'J' in the patellar track. Evidence of quadriceps atrophy and weakness of the hip muscles is partially assessed during the inspection, and partially examined by resistance tests (7, 13). The hip muscles contribute to the alignment of the leg and prevent inward rotation of the leg in stance in knee disease. This inward position can present a risk of recurrent luxation of the knee, as it positions the patella more laterally in relation to the femur (14).

To gather additional information on a possible treatment, patients usually undergo X-ray imaging of their knee to evaluate the presence of trochlear dysplasia, abnormalities in the patellar height and the presence of excessive patellar tilt. Trochlear dysplasia is commonly assessed using the Dejour criteria (15, 16). These criteria are visualised in Figure 5 and include:

- **Crossing Sign:** Indicates abnormal patellar tracking, where the patella crosses the medial border of the trochlear groove. This shows that the deepest point of the trochlear groove crosses the anterior border of the femoral condyles, indicating that the trochlea is not fully developed.
- **Supra Trochlear Spur:** A bone protrusions above the trochlear groove, which can impede proper patellar tracking and contribute to instability.

- Double Contour:** Refers to a second bony ridge or contour present along the trochlear groove, indicating asymmetry of the medial and lateral condyle (hypoplastic medial condyle), which can disrupt smooth patellar movement and lead to instability.

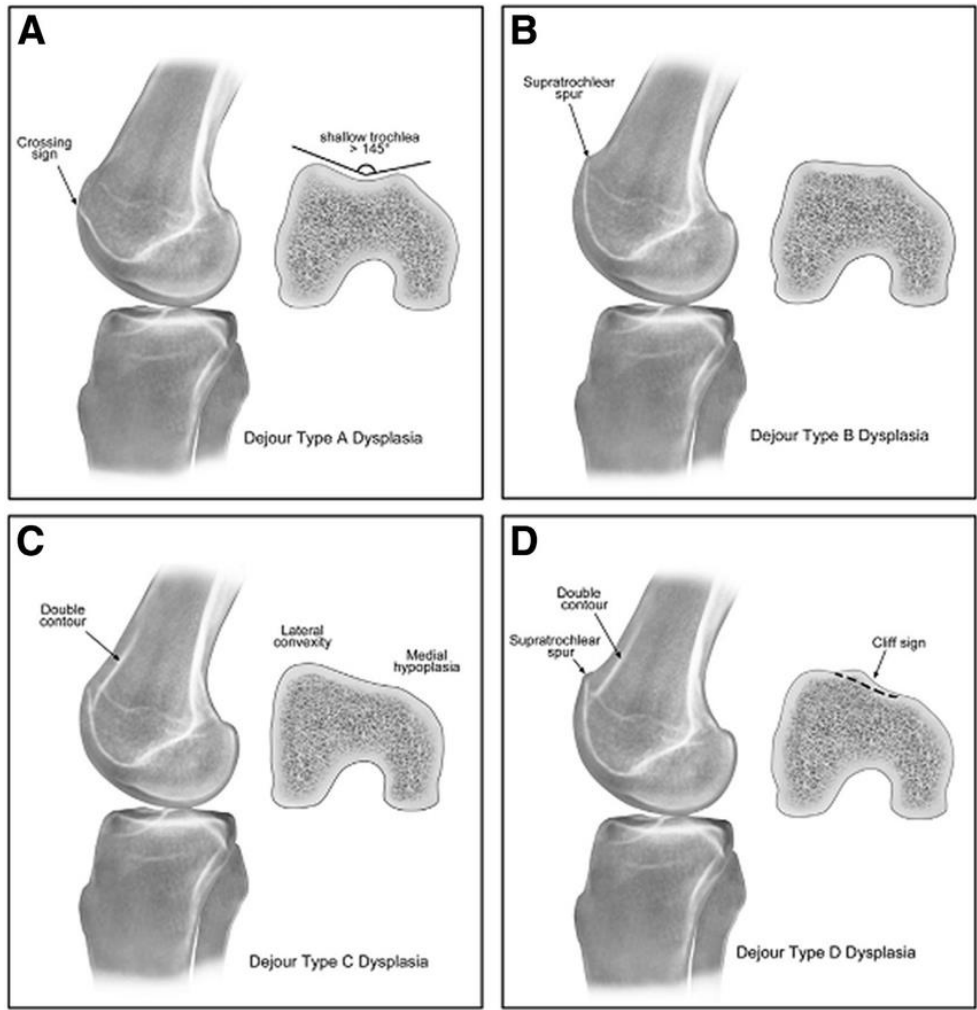


Figure 5: Characteristics of the four Dejour classification categories of dysplasia. The lateral visualisations are commonly used to diagnose trochlear dysplasia using lateral radiographs (17).

Patellar instability can be diagnosed by abnormalities in the patellar alignment. The common parameters to assess this in lateral radiographs is the patellar height index, the Caton-Deschamps index, which is depicted in Figure 6 (18). This ratio can be calculated by dividing the patellar tendon length by the patellar length. An abnormally high ratio of > 1.3 (patella alta) or low ratio of < 0.6 (patella baja) can affect patellar tracking and stability.

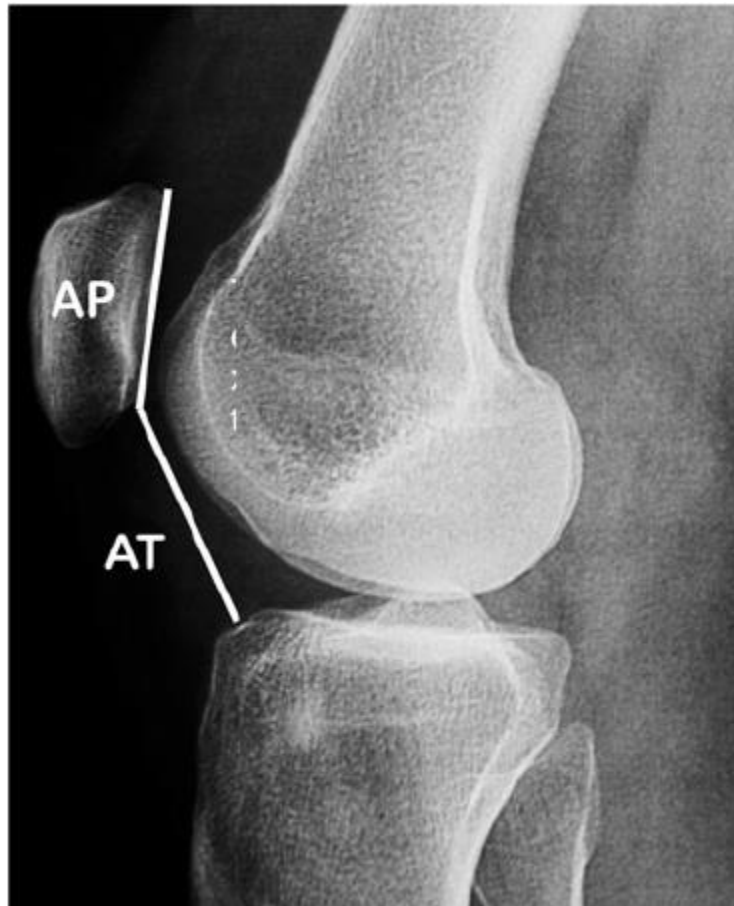


Figure 6: Method to calculate the Caton-Deschamps index via a lateral radiograph, by measuring distance between the anterior angle of the tibial plateau, to the most inferior aspect of the patellar articular surface (AT) and dividing this by the articular side of the patella (AP) (19).

Physical examination gives an impression of the (disturbed) physiology of the knee and imaging gives a two-dimensional (2D) insight into the patient's anatomy. Combined, they determine whether surgery or conservative treatment is necessary and aid in identifying the most appropriate surgical intervention.

2.2.2 Treatment

Conservative methods are often the initial approach for managing PFI after a first dislocation, aimed at improving muscle strength, functional balance, and providing support to the knee joint (10). This can be done through physical therapy, patient education and the use of a patella brace. Specifically, physical therapy plays a pivotal role in this approach, focusing on strengthening the muscles of the leg and hip to enhance stability and correct patellar maltracking. Through targeted exercises and interventions, physical therapy aims to improve muscle coordination and proprioception, ultimately restoring the dynamic balance of the knee joint. Additionally, it is important to address the severity of psychological factors, as losing trust in the knee's stability can lead to avoidance of physical activities, exacerbating muscle weakness and instability over time (20). Therefore, patient education and psychological support are integral components of conservative treatment strategies, fostering confidence and adherence to rehabilitation programs. Lastly, the use of braces can offer external

support to the knee, helping to realign the patella and provide a sense of security and stability to the patient (10). Bracing can be particularly beneficial in cases where there is a loss of trust in the knee's stability, as it encourages patients to engage in physical activities and exercises, preventing further muscle weakness and promoting rehabilitation.

In cases where conservative measures fail to provide adequate relief or stability, surgical intervention may be considered. Several surgical options are available, each tailored to address specific underlying factors contributing to PFI which are diagnosed with physical examination and radiography (17, 21-23):

- **MPFL Reconstruction:** This procedure aims to restore the integrity of the MPFL which is often damaged or stretched in cases of recurrent patellar dislocation. By reconstructing the MPFL, stability is enhanced, reducing the risk of further dislocations.
- **Tibial Tuberosity transposition:** Tibial tuberosity transposition involves realigning the patellar tendon attachment on the tibia to correct patellar maltracking. This procedure is typically reserved for cases of patellar alta or excessive lateralisation of the tibial tuberosity.
- **Trochleoplasty:** Trochleoplasty performed to reshape the trochlear groove of the femur, aiming to address anatomical abnormalities such as trochlear dysplasia. This procedure is complex and delicate, as it involves adjusting the bone structure underneath the cartilage tissue. The surgeon adjusts the bone to create a more congruent trochlear groove, ensuring proper alignment for the patella to track smoothly within the groove. Achieving optimal patellar tracking can be challenging, as it requires precise adjustments to the bone structure under the cartilage tissue to establish stability and reduce the risk of patellar dislocations.

Prior to surgery, patients undergo thorough pre-surgical screening, including imaging studies such as computed tomography (CT) or four-dimensional computed tomography (4DCT) scans, to assess the extent of anatomical abnormalities and plan the surgical approach accordingly. CT imaging offers three-dimensional (3D) insight into the details of anatomical structures such as the trochlea and tibial tuberosity (24). In addition, 4DCT imaging offers also insight into the patellar tracking, offering insight into the dynamic functioning of the knee and the way in which the patellar tracking can be improved (25). Post-surgery, patients undergo a structured rehabilitation program, guided by a physical therapist, to regain strength, range of motion, and function of the knee joint. The first post-operative check with the surgeon typically occurs around six weeks post-surgery, allowing for assessment of healing and progress, and adjustment of the rehabilitation plan as needed. After that, at least one more outpatient clinic visit is planned to follow up with the patient.

3. Technical Background

As described in **Chapter 2**, imaging is one of the components of the diagnostic process for patients with PFI. From the technical medicine perspective, an image is an array of data values which can be used to perform measurements on. Understanding the essence of clinical imaging is therefore important in this thesis and is described in the next section. The second section of this chapter describes how imaging data can be processed for further analysis of this (patient) data.

3.1 Radiography and (4D) Computed Tomography

Radiography and CT are important imaging techniques in orthopaedics due to the high contrast of bones. This is because bones transmit little X-ray radiation and therefore appear white, while soft tissues transmit much X-ray radiation and therefore are (dark) grey (26). One critical factor in X-ray imaging is the transmission angle, being essential for accurate diagnosis. Because trochlear dysplasia can only be assessed when a radiograph is pure lateral (16, 27, 28). Figure 7A-C show the influence of transmission angle on the resulting image.



<p>Figure 7A: This radiograph is not pure lateral (29).</p>	<p>Figure 7B: A second example of a radiograph which is not pure lateral (29).</p>	<p>Figure 7C: A lateral radiograph which is suitable for diagnosing trochlear dysplasia (29).</p>
---	--	---

One critical factor in CT imaging is spatial resolution, which influences scan details and therefore quality (30, 31). Resolution is influenced by parameters such as voxel size, which can be decreased to enhance the image quality and precision of anatomical visualisation. Voxel size refers to the pixel size multiplied by the slice thickness in the image. Additionally, the voltage and current settings in a CT scanner play a crucial role in determining the quality of the images obtained (32). The voltage, in kilovoltage peak (kVp), affects the penetration of the X-ray beam through the patient's tissues. Higher voltages result in greater X-ray penetration, which can be advantageous for imaging deep or dense structures. However, excessively high voltages may lead to increased radiation exposure and decreased image contrast. Similarly, the current, measured in milliamperes (mA), controls the intensity of the X-ray beam. Higher currents produce a stronger X-ray beam, which increases the signal-to-noise ratio and improves image quality. However, higher currents also result in higher radiation dose. By adjusting these parameters, image quality and resolution can be optimised while minimizing the radiation dose to guarantee patient safety. This is crucial not only for clinical diagnosis

and treatment planning but also for research studies seeking to explore subtle anatomical variations and pathologies associated with PFI.

Metal artefacts can significantly deteriorate scan quality, even when the metal is located outside the region of interest (ROI) (33). These artefacts occur due to the interaction between the X-ray beam and metal objects within the patient's body. When the X-ray beam encounters metal implants, such as prosthetic joints or surgical hardware, it undergoes scattering and attenuation, leading to streaks or shadows in the resulting images. These artefacts may obscure anatomical structures and can compromise diagnostic accuracy.

In recent years, the advent of 4DCT scanning has revolutionised the field of musculoskeletal imaging, particularly in the assessment of dynamic joint motion (34-36). By capturing sequential images throughout a range of motion, 4DCT scans provide insights into kinematic abnormalities associated with conditions like PFI. This dynamic imaging modality offers clinicians a deeper understanding of joint mechanics, improving the diagnosis and treatment planning.

3.2 Image Processing

In order to analyse 3D structures within a CT scan, bones need to be converted into meshes by segmentation. This segmentation task is accomplished using a 3D U-Net algorithm specifically trained for knee CT data. The resulting segmentation mask represents a binary image where the pixels corresponding to the knee bones are assigned to a specific class, while background pixels are assigned a value of 0. Once the segmentation mask is obtained, it is imported into MATLAB (MathWorks, version R2023B) for further processing. MATLAB provides tools for mesh generation and optimisation. The segmentation mask is transformed into a surface mesh consisting of vertices and faces. Vertices are points in 3D space that define the corners of geometric shapes, while faces are formed by connecting vertices to create polygonal surfaces. Mesh quality is influenced by the density of the vertices, an increased density generally results in a more detailed and accurate representation of the knee bones. However, excessively dense meshes can lead to performance problems due to computational intensity and high memory usage, thereby impacting the efficiency of subsequent analyses.

3.3 Statistical Shape Modelling

A Statistical Shape Model (SSM) is a mathematical representation of shapes based on statistical principles, enabling researchers to quantify and compare shape variations (37). In orthopaedic research, statistical shape modelling plays a crucial role in analysing anatomical structures, understanding deformities, and aiding in surgical planning (38). By creating SSMs from medical imaging data such as CT scans, researchers can investigate differences in bone morphology among a group of individuals, assess the progression of diseases like osteoarthritis, and evaluate the outcomes of orthopaedic interventions.

To build a SSM, first, 3D imaging data is acquired of the objects or anatomical structures of interest (37). This data can be obtained from modalities such as CT or surface scanning techniques. The acquired data undergoes pre-processing steps to enhance its quality and suitability for further analysis. This may involve noise reduction, image segmentation to isolate the ROI, and surface reconstruction to generate a geometric representation of the object (37). Common representations

include boundary representations (e.g., point clouds, mesh surfaces) or volumetric representations (e.g., voxel grids).

Establishing correspondence among the geometric representations in the dataset is crucial for creating a coherent statistical model. Correspondence ensures that points on different shapes represent anatomically equivalent locations. Various techniques such as landmark-based methods, surface-based registration, or feature matching algorithms can be used to establish correspondence (37). Once the corresponding points are found, analyses can be performed on the dataset. This is commonly executed by a principal component analysis (PCA), which identifies the principal modes of variation present in the dataset by decomposing the covariance matrix of shape coordinates (39). Each principal component captures a distinct pattern of shape variation, ranging from global size and orientation changes to localised deformations. Using the identified principal components, a SSM is constructed, which is calculated by averaging each corresponding point across all shapes in the dataset (37). This model represents the mean shape of the population, along with variations captured by the principal components. By combining the mean shape with weighted combinations of principal components, new shapes within the population can be interpolated.

In this research, ShapeWorks (40) will be used to create a mean model of asymptomatic and healthy femurs, patellas and tibias. ShapeWorks is software, specially created for such purpose. It enables to import 3D data, as meshes, in order to process and analyse this.

4. Introduction to this Research

Patellofemoral instability (PFI) is a condition in which the patella dislocates from its normal anatomical position within the trochlear groove (7). This instability can lead to symptoms including pain, functional limitations, recurrent instability and increases the risk of osteoarthritis (7, 41). Trochlear dysplasia plays a significant role in the onset of PFI, as it obstructs the trochlea's ability to provide adequate support and guidance for the patella, thereby increasing the risk of dislocation (13, 15, 16, 27, 28). Yet, the precise correction of trochlear dysplasia is uncertain (42).

It is common in orthopaedic surgery to use the contralateral bone as a reference for surgical anatomical alignment, to quantify pathologies and to use for reconstruction (43-46), but a morphological 3D analysis is not yet performed concerning the degree of symmetry between knees. This raises questions about the pre-operative planning of PFI surgery, because PFI patients may develop symptoms unilaterally or bilaterally and it is not evident whether knee morphology is related to this development. A previous study highlighted disparities in trochlear dysplasia severity between contralateral and ipsilateral knees in patients with unilateral patellar dislocation, as measured by linear trochlear inclination and Dejour criteria (47). This study was executed with 2D landmarks of the knee in multiple planes. The results of this research contrast with earlier observations in healthy knees, suggesting that side-to-side differences in patellofemoral anatomical risk factors were clinically insignificant in asymptomatic individuals. Another study has been conducted that examined the morphological symmetry between the tibial plateau (46). In this research, this comparison was performed with 3D meshes, with the outcome leading to a high degree of symmetry. This study has not yet been performed for other parts of the tibia and for the other bones of the knee. Therefore, there are several studies that conclude a degree of bilateral asymmetry in PFI/healthy knees, but no study has been conducted that examines this for all three bones at the morphological 3D level.

A study conducting 3D analysis on the morphological bilateral symmetry between (PFI) knees can provide insight on the shape of bone components in more detail than in 2D analyses or those that rely on parameters. Given that treatment in clinical practice considers a 3D perspective, understanding the degree of symmetry between knees becomes crucial for guiding treatment decisions. With this research, more knowledge is gained about the 3D anatomy of the knee, assessing the degree of morphological bilateral symmetry. Based on the results of this study, it can be determined whether the contralateral side can be used as a surgical reference in PFI surgery, as trochleoplasty. Thereby, the influence of morphological symmetry on the bilateral symmetric motion of PFI knees can be investigated. After all, PFI is also a dynamic problem, where conclusive information about the bilateral symmetry of the knee could provide more answers about the origin of (uni- and bilateral) dynamic complaints. Concluding, this study provides fundamental insights into the degree of morphological bilateral symmetry and therefore the 3D anatomy of the knee, which can be further built upon in multiple branches of research.

5. Research Objectives

There is fundamental uncertainty in the literature regarding the degree of morphological bilateral symmetry of the bones of the knee. The answer to this uncertainty may provide a basis for further research on PFI and trochlear dysplasia. Therefore, the following research goals were formulated:

Main goal

Investigate the degree of 3D morphological bilateral asymmetry of the bones comprising the knee joint, including the femur, patella, and tibia.

Sub-goals:

- To investigate to which extent and in which regions healthy knees exhibit morphological bilateral asymmetry.
- To examine to which extent and in which regions knees with mild and severe trochlear dysplasia demonstrate greater/less morphological bilateral asymmetry compared to healthy knees.

6. Materials & Methods

In the following flowchart, the method of the research is visualised. Each component of the flowchart (Figure 8) is described in **Sections 6.1 – 6.6**.

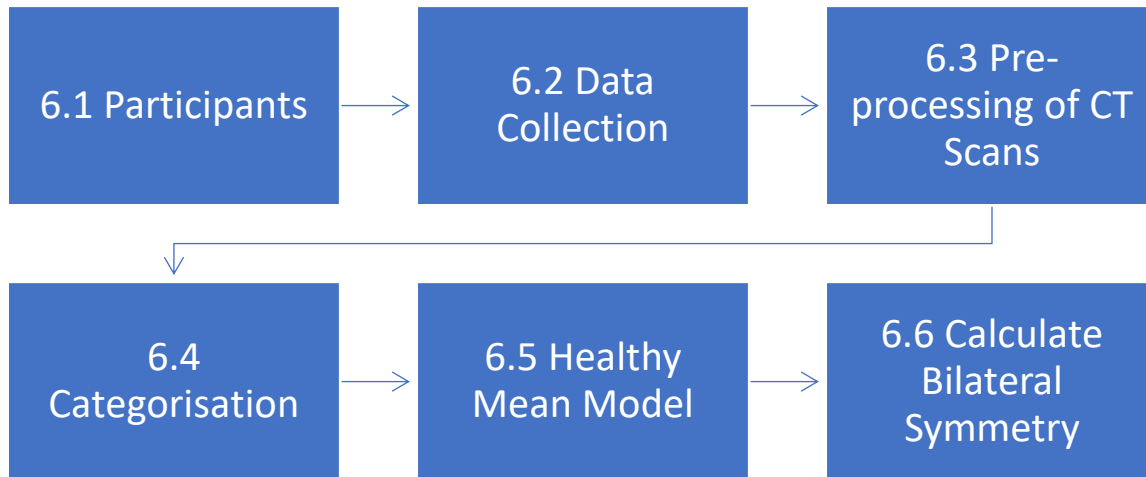


Figure 8: A pipeline which shows the components of the method section.

6.1 Participants

This examination was performed using CT images depicting both knees. The CT scan date was set within the period of 11-2013 until 11-2023, to compile a comprehensive dataset, while also excluding scans subjected to outdated scanning protocols to maintain relevance. The age of the patient at the time of the scan was set between 16 and 40 years, to prevent the presence of osteoarthritis. Finally, it was specified which parts of the bones of the knee joint should at least be on the scan (distal femur with condyles, trochlea and including the metaphysis, patella completely and proximal tibia including the metaphysis with the tibial tuberosity). These bones should show the original anatomy and thus should not be morphologically affected by surgery or pathologies as osteoarthritis, osteonecrosis, fractures, cysts or tumours. The minimal resolution was set at 1 mm, enabling capturing left-right differences of 1 mm.

6.2 Data Collection

Using the in- and exclusion criteria, data was obtained in two ways. Firstly, available data from existing databases was used consisting of knee CT scans of 100 healthy volunteers, 43 patients known to have PFI and 19 patients known to have PFP. Additionally, 2 static scans of healthy volunteers were available. The static scans were relevant for the purpose of this study.

Secondly, a new data request was performed using CliniQuest by building a CliniQuery to obtain CT scans. After setting requirements, based on the description in **Section 6.1**, there were 1167 hits

regarding the number of patients who had scans in the database with these requirements. The CT scans of these patients were requested. In case of multiple CT scans from one participant, only the earliest scan was included. Radiographs were additionally requested, in order to be able to categorise the data by the Dejour criteria.

After this request, a list with data of the CT scans was issued. This list originally contained 1167 unique patients. After this filtering by pathologies which complied with the exclusion criteria of **Section 6.1**, this was reduced to 1027. The radiography list originally contained 1680 unique patients. This has been reduced to 370, which means that of the 1027 patients 370 also have a matching radiograph.

Two separate lists of CT and radiography with all patient numbers, accession numbers and scan dates were submitted to the radiology and nuclear medicine department of Radboudumc. All data were anonymised, to guarantee the privacy of the patients and subsequently stored on a shared drive of the orthopaedic research lab at Radboudumc, only accessible to those involved in this study.

The CT data was rescreened using the inclusion and exclusion criteria. All CT scans were opened and assessed whether both knees were visible on the CT and whether they were suitable for inclusion in the study. The total in- and exclusions of CT scans is visualised in the flowchart of Figure 9. The radiography list originally contained 1680 unique patients. 28 of these patients were ultimately included and therefore have a matching radiograph. These radiographs were examined to determine whether a lateral radiograph of both knees was available. These were checked again for the inclusion and exclusion criteria, because these radiographic images were often not made on the same day as the CT images and therefore a different medical situation could apply to the patient when the radiography was made. This could influence the assessment of the inclusion and exclusion of the radiographic scan. Radiographic scans showing surgical marks or other impairment of the anatomy, were not used further in the study.

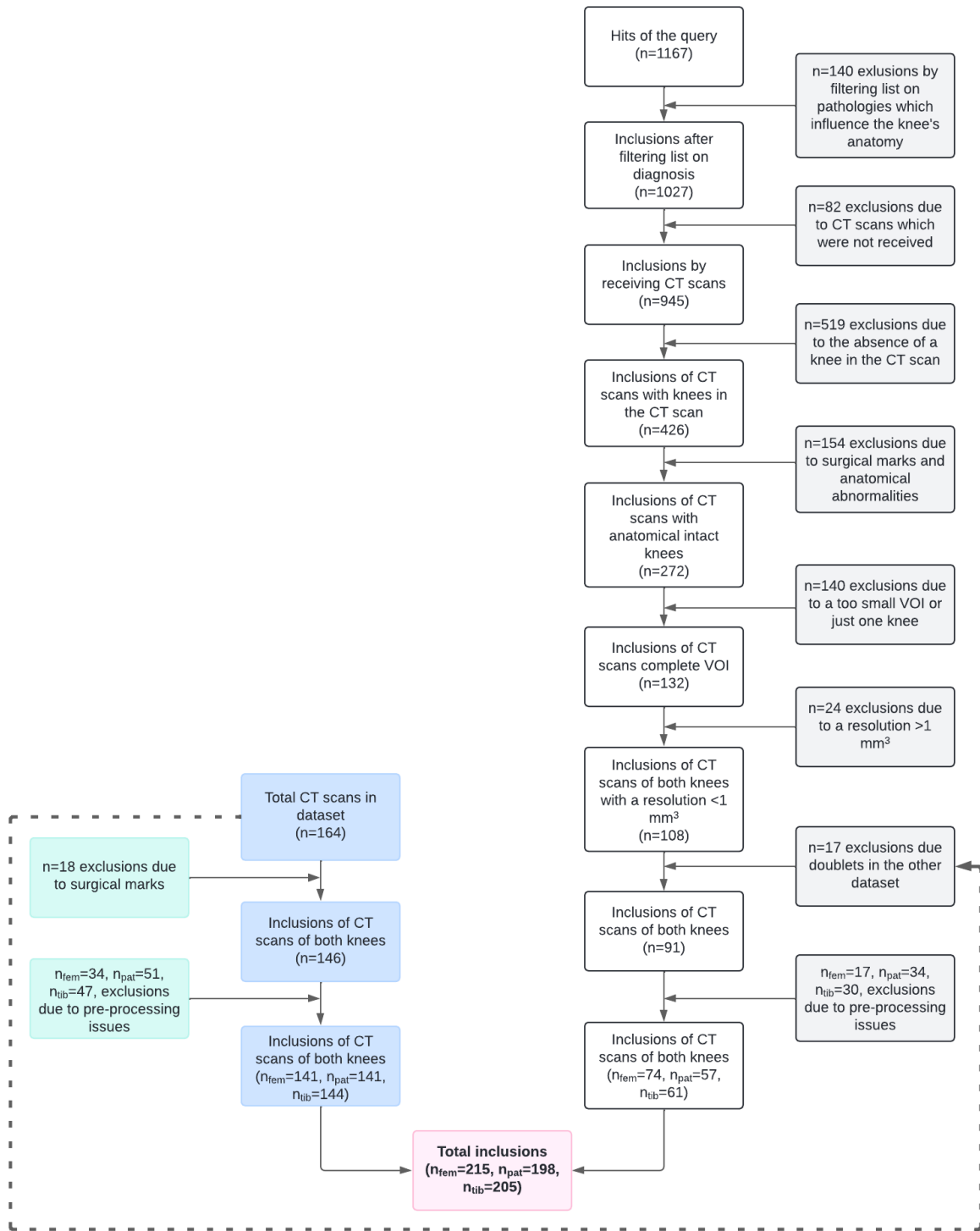


Figure 9: Total of in-and exclusions of CT scans.

6.3 Pre-processing of CT Scans

The requested CT data is not prepared to perform morphological analyses with it yet. Pre-processing steps were needed to prepare data for 3D analyses. The following steps were performed on the CT scans to convert them into meshes that were used to analyse morphology (Figure 10):

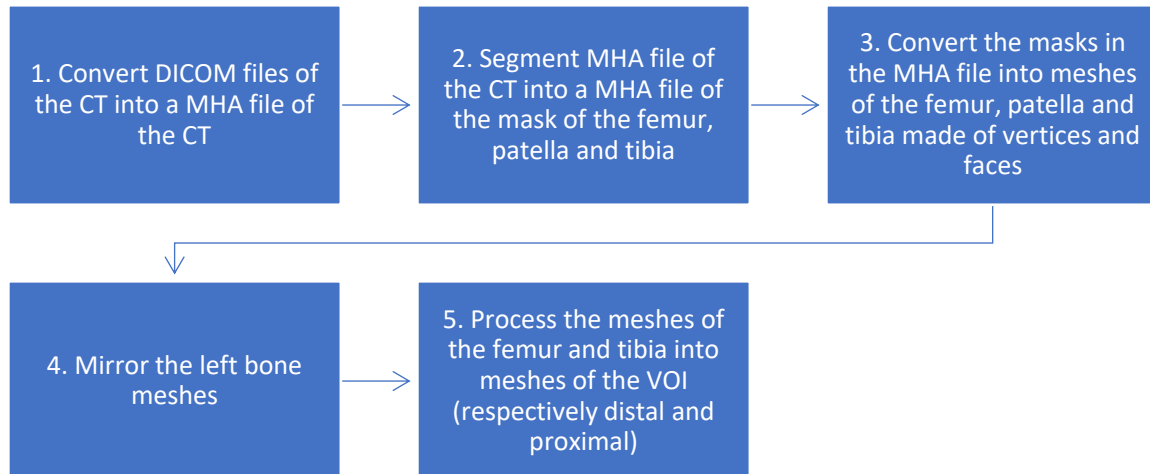


Figure 10: A pipeline which shows the steps of converting a CT scan into meshes.

The steps in this pre-process are explained further in this section.

1. The CT data was provided in the form of multiple DICOM files. To segment the data in step 2, they need to be converted to an MHA file. Here, the DICOM files are converted using a Python (Python version 3.12) code from the orthopaedic research lab. This code read the DICOM series within each subfolder using ImageSeriesReader from SimpleITK (an image processing toolkit for Python) (48). Various properties of the DICOM series were obtained, such as origin, spacing, direction, and size. Then, the image was saved as MHA file.
2. The MHA file contained CT data, however, this data was not suitable for the morphologic analysis. The data was segmented to obtain a 3D representation of the three bones of the knee (femur, patella and tibia). Segmentation of this data was done by means of a nnU-Net (49) trained at the orthopaedic research lab. The average Dice coefficients were of the femur 0.998, of the tibia 0.981 and of the patella 0.972 (25).
3. From the data stored in the masks, 3D representations were created in the form of meshes. The MHA volume was read using the MATLAB code provided in **Appendix A1**, obtained from the orthopaedic research lab. Subsequently, meshes were created for each left and right bone (femur, patella, tibia) from the MHA volume using morphological operations as dilatation and erosion. The number of vertices was set to 10,00 for the femur and tibia and 5,000 for the patella.
4. The fourth step included mirroring the left meshes, which was essential in order to be able to compare the left and right mesh per bone component (Figure 11). Mirroring was done using

a MATLAB code which can be found in **Appendix A2**. The following calculation shows how the mirroring of the vertices in the x-direction with a reflection matrix was executed:

$$\text{left vertices} * \begin{bmatrix} -1 & 0 & 0 \\ 0 & 1 & 0 \\ 0 & 0 & 1 \end{bmatrix} = \text{mirrored vertices}$$

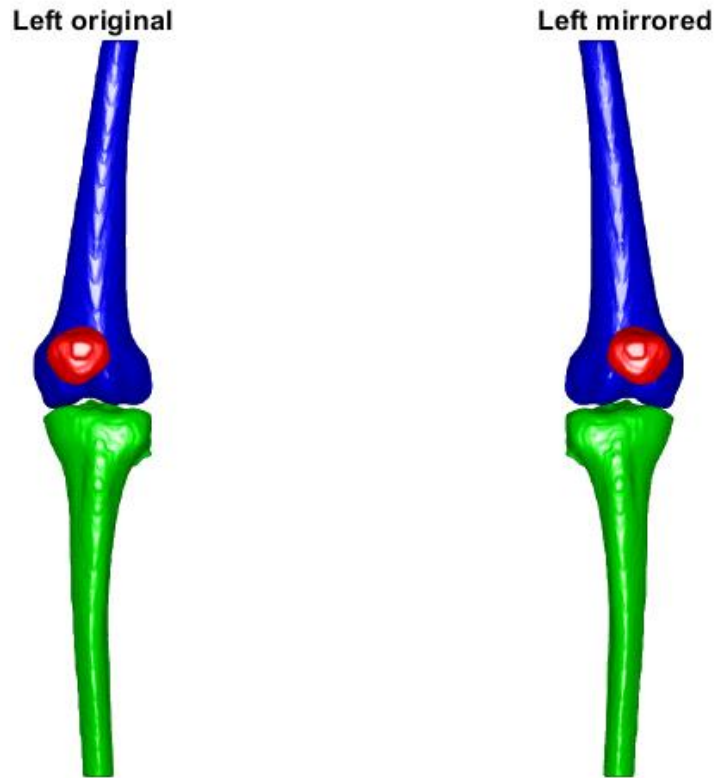


Figure 11: Mirroring the left bone meshes in MATLAB.

5. This step cut the bone meshes of the femur and tibia to only get the volume of interest (VOI) (**Appendix A3**). The VOI of the patella is the entire bone, so this bone did not need further processing in this step. The VOI of the femur is the distal epiphysis and the diaphysis. To define this VOI, the width of the bone was determined in the x-direction (medial-lateral) and this dimension was used as the cut-off height in the z-direction (proximal-distal). This made the width in the x-direction the same as the height in the z-direction. The cutting is visualised in Figure 12A and B. The mirrored patella meshes and mirrored and cut femur and tibia meshes were saved as STL and MAT files.

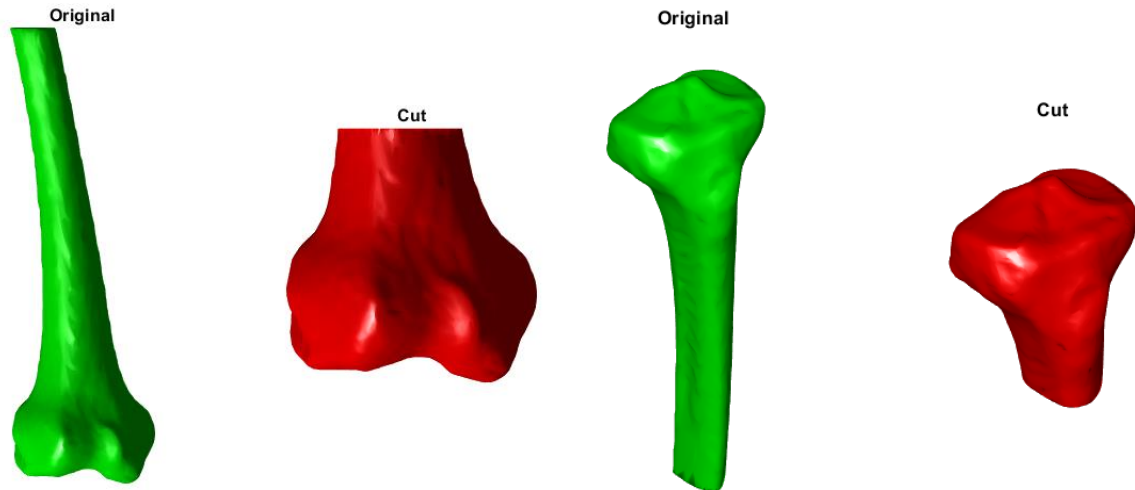


Figure 12A: Cutting the femur mesh in MATLAB.	Figure 12B: Cutting the tibia mesh in MATLAB.
---	---

6.4 Categorisation

All groups were categorised into no dysplasia, mild dysplasia (Dejour type A) severe dysplasia (Dejour types B, C and D). This was done to prevent the groups with dysplasia from being too small. According to a previous study, it is valid to make this division from four to two groups (50).

Trochlear dysplasia was determined in three manners. Firstly, the individuals which had a matching lateral radiograph of both knees were categorised on these radiographs. Secondly, for those individuals without a radiograph, artificial lateral radiographs are made from the CT images with the MATLAB code provided in **Appendix A6**. Parts of this code were obtained from the orthopaedic research lab. The code aligned the bones according to the European Research Community (ERC) Knee Reference Frame and subsequently rotated the knee to obtain a lateral projection. This results in simulated radiographic images of the right and left knee of each individual. This code did not work for all knees included in the study, because using the ERC Knee Reference Frame required a larger part of the femur than for inclusion in the study. As a result, CT scans were included for which the femoral component was too short to make this calculation. The rotations were not calculated correctly, so this did not result in a lateral radiography. Therefore, the third categorisation method was to determine the trochlear dysplasia was determined with the whole CT scan.

All Dejour classifications were made by an orthopaedic surgeon dr.ing. S.A.W van de Groes, who is involved in this research and is specialised in knee pathology. The order of the images was randomised, so that the left and right knees of an individual would not follow each other. The orthopaedic surgeon was not aware of any patient information during the assessment, in order to make the assessment as objective as possible. In the same categorisation session, eleven individuals were assessed a second time by the surgeon to get an indication of the consistency in the orthopaedic surgeon's assessment. This score was seven out of eleven double categorisations.

Two of the radiographic images could not be assessed due to poor image quality. It was decided to assess this on the basis of the CT scan. For 9 individuals, only one side (left or right) could not be properly assessed due to the poor quality of the radiograph. These were classified in the category of

the contralateral side. Individuals in whom the left side was not rated the same as the right side were assigned to the group of the side with the highest dysplasia rating.

Of the data available from previous research, 41 individuals had already been assessed for trochlear dysplasia, by the same orthopaedic surgeon. The individuals for whom the group was already known were not included in the assessment a second time.

6.5 Healthy Mean Model

To calculate the degree of bilateral symmetry of the knee, it was important to have corresponding points for each bone component that can be compared. This allowed data from large groups of bone components to be merged and the degree of symmetry there was determined for each point per individual and group. This required a mean model of the bone components, because this could be used in registration, to work with the same number of vertices located at the same position on a bone at each registration.

The mean model was created using the ShapeWorks software. To create an overall picture of the bone compartments, mean models of the femur, patella and tibia were made of the compartments belonging to the group without trochlear dysplasia. Those meshes were remeshed in order to create a surface with the same number of vertices. This was 11,019 for the femur, 3,006 for the patella and 8,018 for the tibia. The number of vertices determined the number of distances that can be calculated over the surface. The mean model was then calculated averaging 1,000 and for the patella 500 particles spread over the surface of the bone. The resulting mean bones are visualised in Figure 13A-C. These mean models were exported as STL- to be used in MATLAB. The exact settings of the software can be found in **Appendix B**.

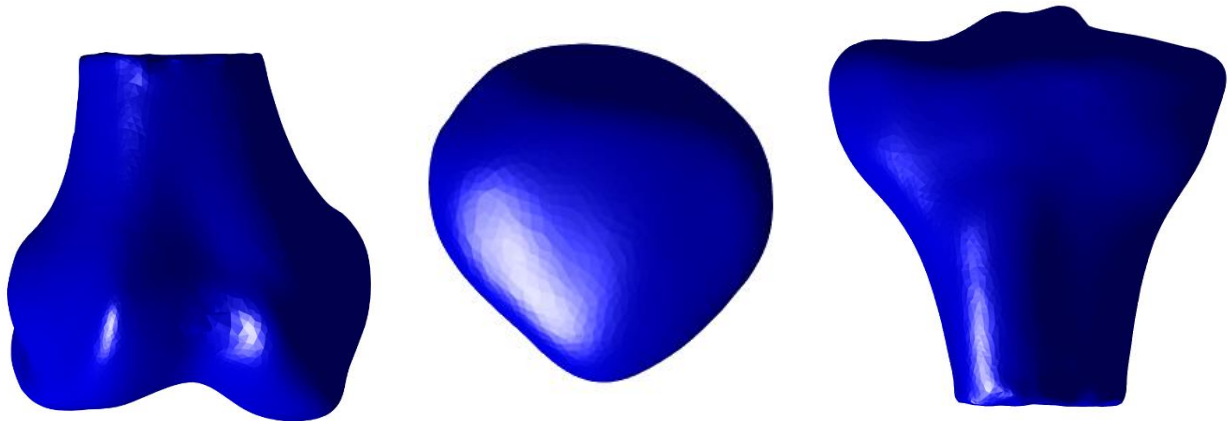


Figure 13A: Mean model of the femur.

Figure 13B: Mean model of the patella.

Figure 13C: Mean model of the tibia.

6.6 Creating Regions

To be able to assess the degree of morphological bilateral symmetry in regions of the three different bone components, a regional division was made based on the formed mean bones. The regions were based on the bone's anatomy and how the anatomy is related to PFI or trochlear dysplasia. The areas are shown in Figure 14A-C.

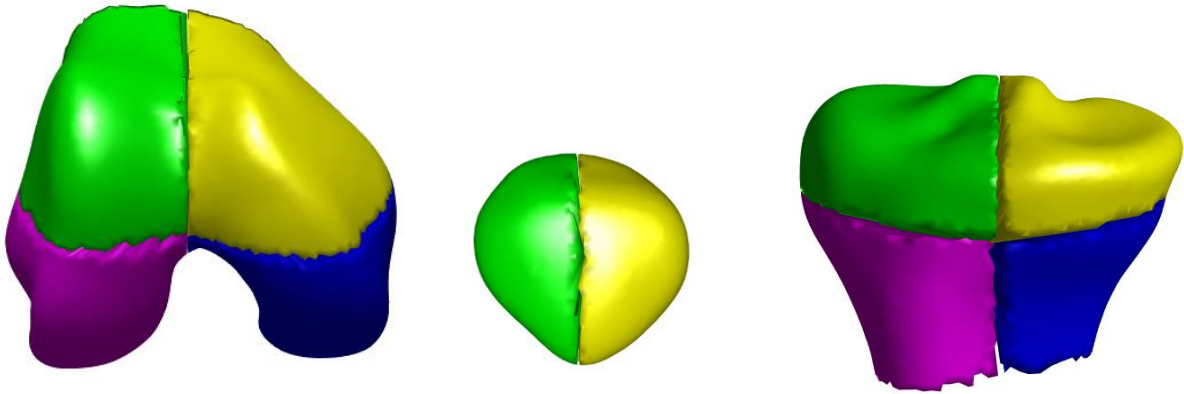


Figure 14A: Regions of the femur.	Figure 14B: Regions of the patella.	Figure 14C: Regions of the tibia.
-----------------------------------	-------------------------------------	-----------------------------------

For the femur, a division was chosen between an anterolateral and anteromedial part, and a posterolateral and posteromedial part. This approach was selected to examine the lateral and medial condyles of the femur as regions of interest, where the anterior part primarily provides information about the parts of the condyles influencing the trochlea. These areas are therefore of great interest for investigating the development of dysplasia and whether this condition develops bilateral symmetrical. Examining the posterior regions provided information about the posterior side of the two condyles and the degree of morphological bilateral symmetry on this side. The condyles are interesting to investigate because the size of the condyles may depend on trochlear dysplasia, with the medial condyle usually being hypoplastic (51, 52). The upper 20 mm of the vertices of the femur are not included in the regions, to prevent the influence of overestimating the distances due to cutting artifacts. This exclusion of vertices is visualised in Figure 15A and B.

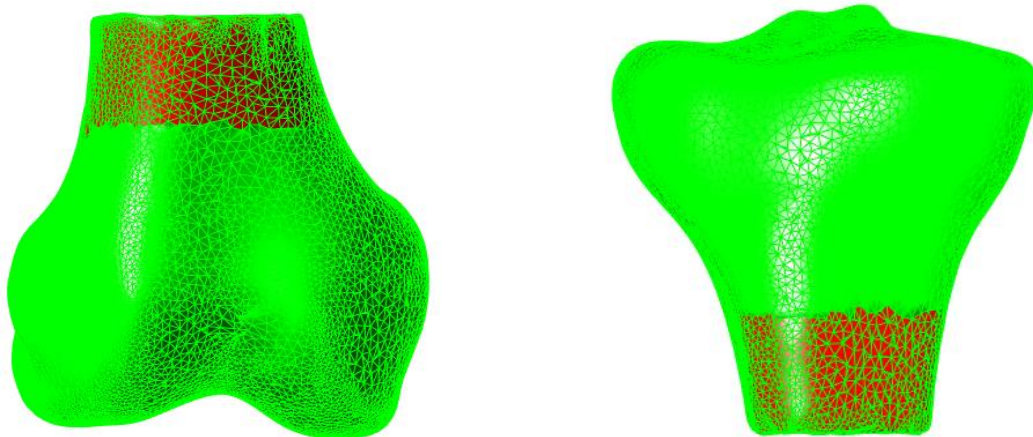


Figure 15A: Exclusion of the proximal 20 mm of vertices in the femur bone part.	Figure 15B: Exclusion of the distal 20 mm of vertices in the tibia bone part.
---	---

The patella was divided into a lateral and medial region to investigate whether there was a difference in the degree of symmetry in these areas. A lateral-medial division was chosen because it was known

that the development of the patella's shape is associated with the development of the trochlea's shape (53). Therefore, this division could potentially reveal symmetry difference in cases of trochlea dysplasia.

For the tibia, a division was made into a lateral and medial area of the tibial plateau and a lateral and medial area below the tibial plateau, at the level where the tibial tuberosity is located. The tibial plateau was divided laterally-medially because this area comprises medial and lateral articular facets separated by a central intercondylar area. Thereby, the lateral posterior tibial slope was found to be flatter for patients with trochlear dysplasia than healthy subjects (54) and the medial tibial slope is greater for patients with trochlear dysplasia than healthy subjects (55). The area below the tibial plateau followed the same lateral-medial division, as this is where the tibial tuberosity is located, and the position of this bone part can be lateralised in cases of PFI. Because the tibial tuberosity was in one region in this division, this region could be compared with the one without this bone component. The lower 20 mm of the vertices of the tibia are not included in the regions, to prevent the influence of overestimating the distances due to cutting artifacts.

Because the regions of the bones were based on the vertices of the mean models, 2 or 4 groups of vertices were formed per bone. This allowed for not only a general bilateral comparison per individual but also a bilateral region comparison. Subsequently, it was possible to investigate within each group whether specific regions were significantly more (a)symmetrical than other regions.

6.7 Calculate Bilateral Asymmetry

In this final step, the distances between the surfaces of the left and right bone components of the femur, patella and tibia were calculated in two main steps. In the first step, the mean model created in **Section 6.5** was registered on both the left and right bone components, with the code described in **Appendix A4**. In the second step, the registered mean model was morphed on these two components. This caused the shape of the mean model to change to the shape of the bone component. The vertices of the mean model were registered to the surface of the bone individual components, for both the left and right side. This allowed measurement of the absolute distance between each corresponding vertex of the left and right bone which could be assumed as the degree of asymmetry per individual. Figure 16 provides insight in these steps.

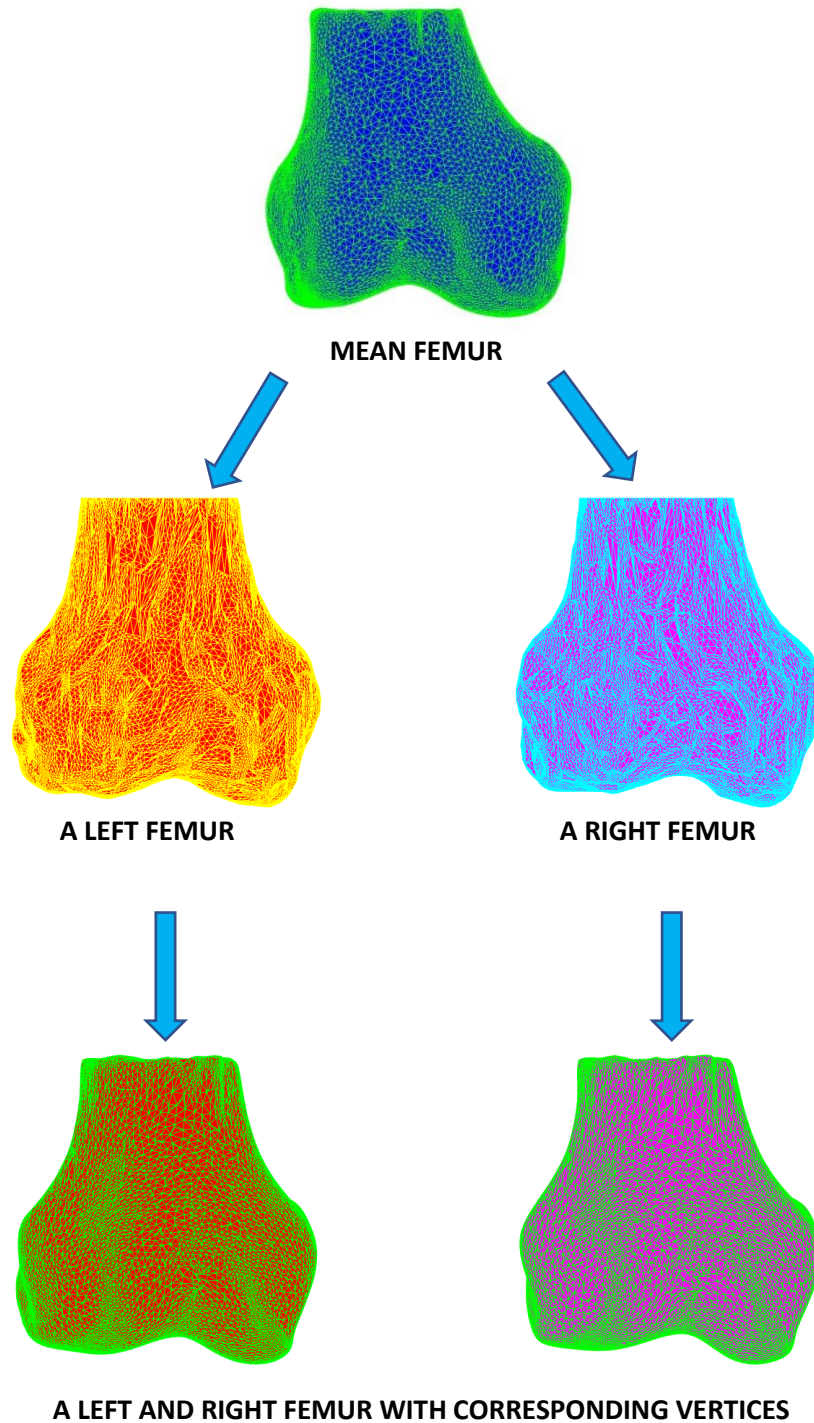


Figure 16: The function of the mean bone as template to create corresponding vertices between the left and right bone, in order to calculate the bilateral asymmetry.

Since the vertex location corresponds for all individuals, conclusions can be derived about the degree of symmetry for each group. For the femur, the upper 20 mm of distances were not included in the calculations, to prevent overestimating the distances due to cutting artifacts. For the tibia, this was lower 20 mm. By converting the distances to a colour scale, the symmetry can be visually displayed

per bone component per individual and per group. The colour maps were made with the code in **Appendix A5**.

7. Results

This results section is divided into two parts to achieve the two sub-goals of this study. Together, these sub-goals result in the main research goal 'Investigate the degree of 3D morphological bilateral asymmetry of the bones comprising the knee joint, including the femur, patella, and tibia'.

7.1 Sub-goal 1

Sub-goal 1 is: Investigate to which extent and in which regions healthy knees exhibit morphological bilateral asymmetry. For this, the results of the group without trochlear dysplasia follow in this section. The results show visually and quantitatively the degree of morphological bilateral asymmetry and where the asymmetry is localised in each bone.

7.1.1 Visualisations

To provide insight into the degree of morphological bilateral asymmetry, 3D colour maps are incorporated in this section. Figure 17 shows an example of how a colour map is formed for one individual.

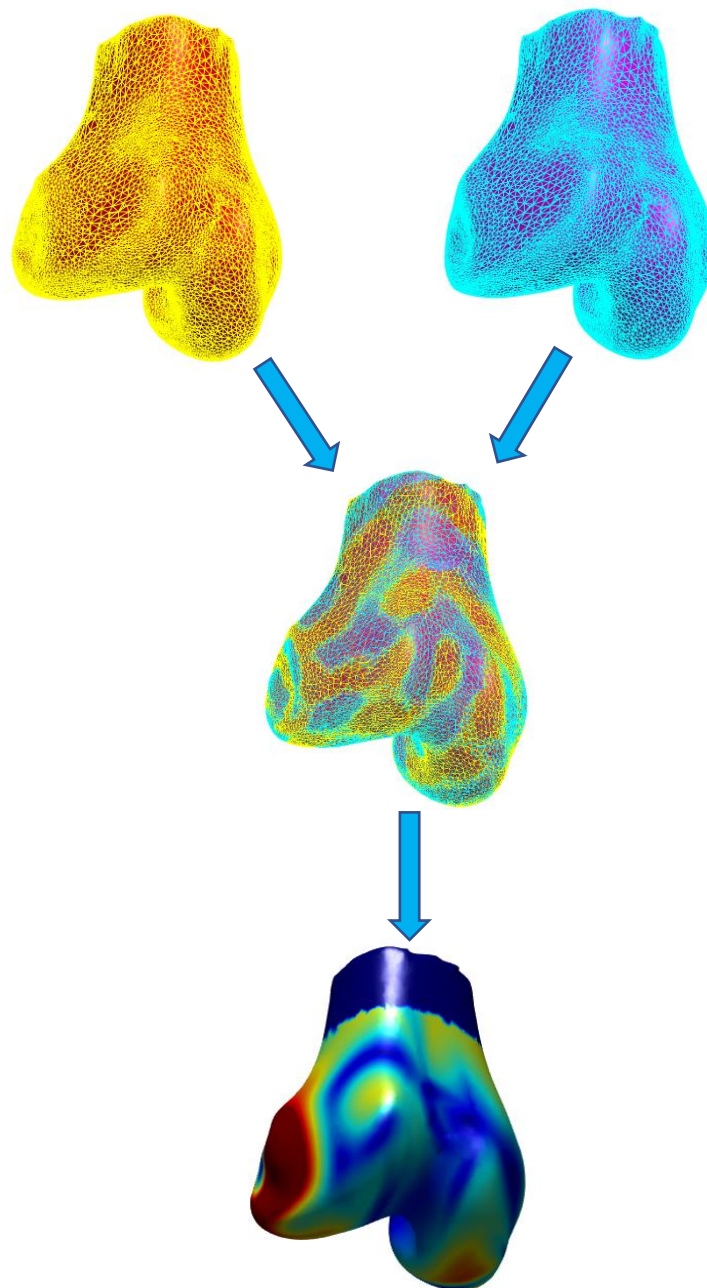


Figure 17: A representation of the calculation of surface distances between a left and right femoral component, and how this results in a colour map.

In Figure 17 it can be seen that the locations on the femur that are clearly different between left and right are also highlighted in the colour map. So, the more red the location is in the colour map, the greater the degree of asymmetry is. Because this calculation was made for all bones, the median for each vertex can be calculated. This makes it clear what the degree of morphological bilateral asymmetry is for the whole group by location in the bone. A median is suitable in order to represent

data of the group, because the data is non-symmetrically distributed and outliers exist in the data. This was assessed with histograms. The histogram of all data is visualised in Figure 18.

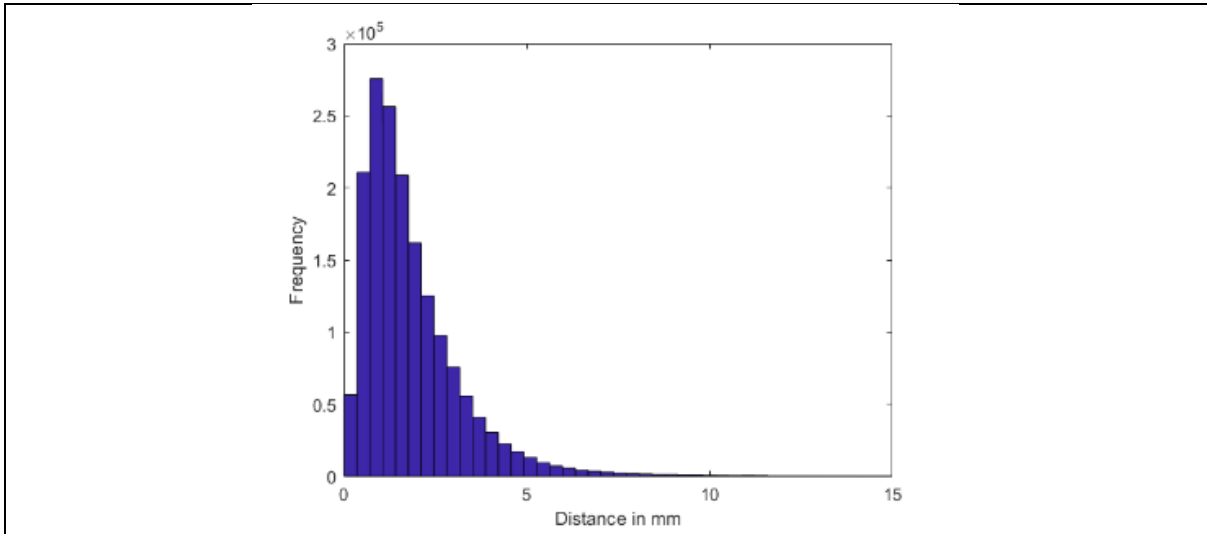


Figure 18A: Histogram of the data of the femur of group o.

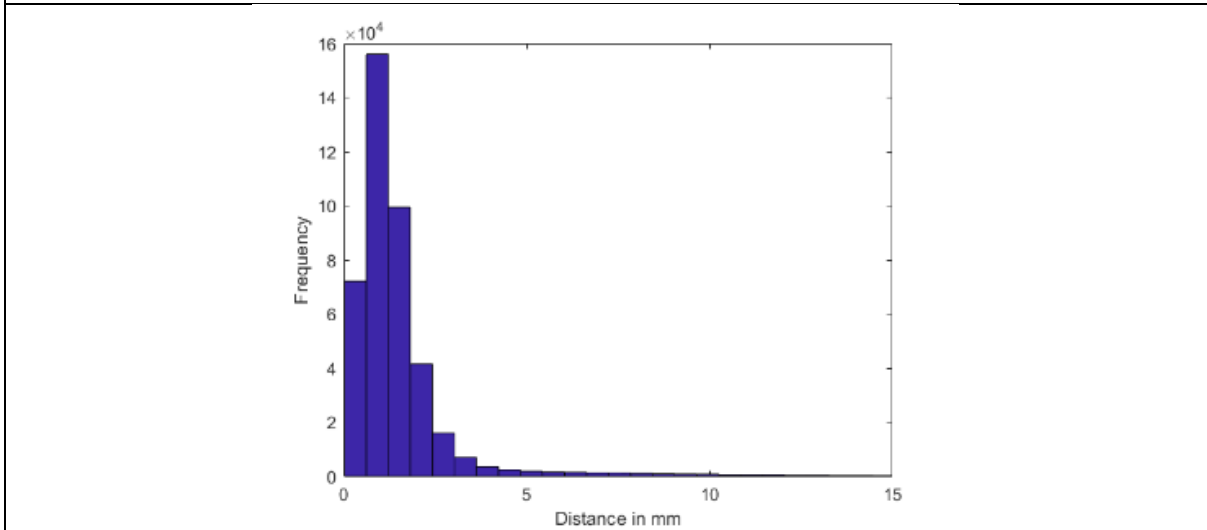


Figure 18B: Histogram of the data of the patella of group o.

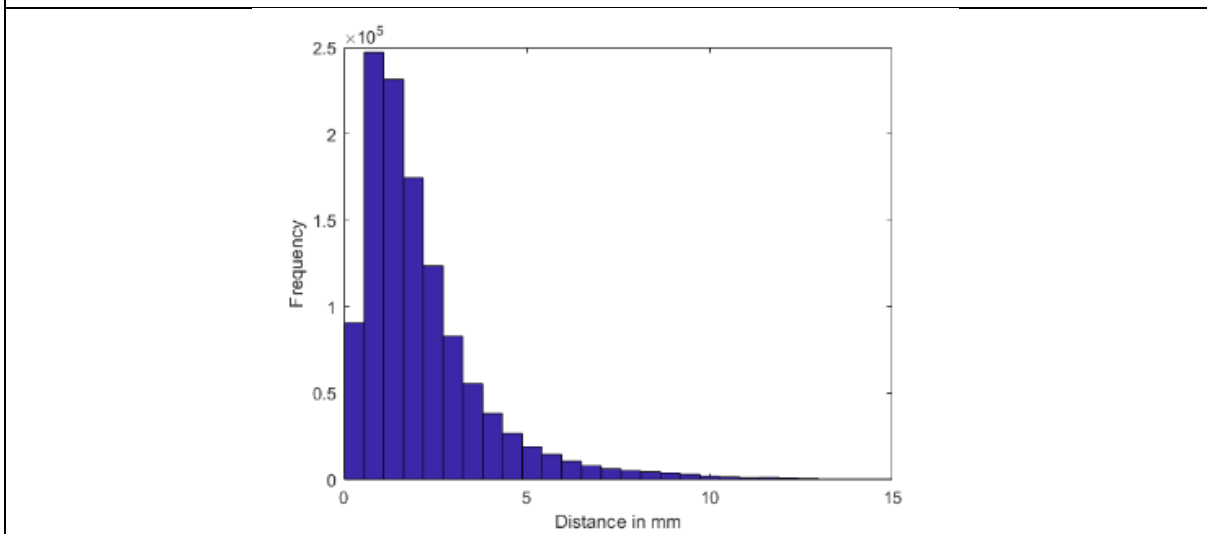
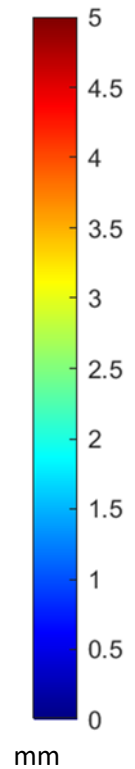
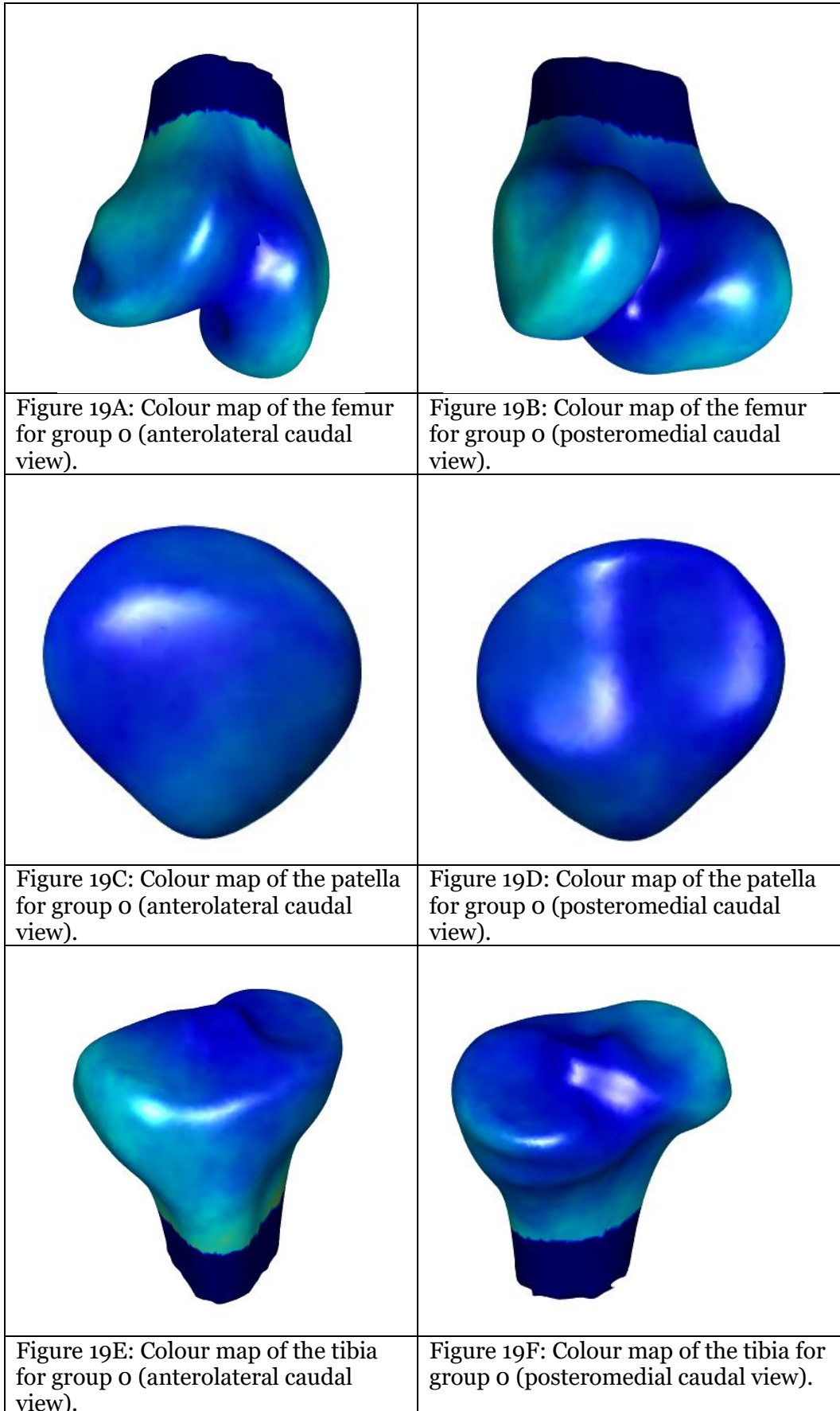


Figure 18C Histogram of the data of the tibia of group o.

The medians per vertex are shown in the colour maps in Figure 19A-F. The figures are made at specific angles, providing a better view of the joint surfaces.

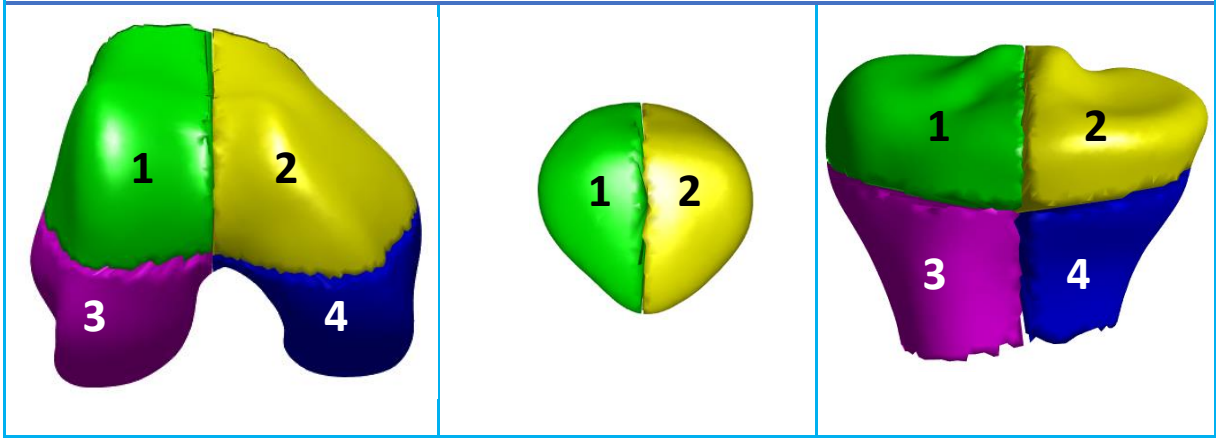


Visually, there is little highlighted in these colour maps. For the visualisation of the femur, the lateral and medial part present the most bilateral asymmetry. The patella does not present any highlighted locations. For the tibia, the anterolateral part is highlighted the most.

7.1.2 Quantification

Table 1 displays of the degree of morphological bilateral asymmetry per bone region, as described in Section 6.6. This is expressed as the median together with the interquartile range (IQR), which describes the boundaries between the lowest 25%, the middle 50% and the highest 25% of all data.

Table 1: Median and IQR in mm for the femur, patella and tibia, for group 0, for the total bone and for the regions.



Bone	Group	Total bone	Region 1	Region 2	Region 3	Region 4
Femur	0 (n=154)	1.3 ± 0.7	0.6 ± 0.1	0.6 ± 0.2	0.5 ± 0.3	0.5 ± 0.3
Patella	0 (n=138)	0.9 ± 0.2	0.8 ± 0.2	1.0 ± 0.2		
Tibia	0 (n=144)	1.4 ± 0.8	0.7 ± 0.4	0.5 ± 0.2	0.8 ± 0.2	0.7 ± 0.2

The results in Table 1 show asymmetries for group 0 around 1 mm.

7.1.3 Statistics

To achieve the sub-goal, that is, to know which regions in the healthy bone models show asymmetry, it is important to investigate which bone regions are significantly more asymmetric than others. For this, mixed model analysis is a suitable statistical method. This statistical method is applied to datasets with hierarchy and interdependencies. In this case, the hierarchy in the data is as follows: the data is divided into a group (group 0, 1 and 2). Individuals are assigned to these groups. These have for the femur and tibia four, and for the patella two regions with vertices over which surface distances were calculated to determine the degree of asymmetry. The order is thus *group > individual > region > vertex > distance*. A mixed model consists of fixed and random effects. Fixed effects represent the overall average effects that are consistent across all groups or levels. These effects are of primary interest and can be directly interpreted. In this case, the groups and regions are fixed effects. There are no interdependencies between the groups and regions or random deviations to consider. Random effects account for variations that are not captured by the fixed effects, representing random deviations from the overall averages. The random effects are the individuals and the vertices, because the distances in general may be increased for an individual, and therefore linked to this. The vertices are a random effect, because each vertex is at a corresponding anatomical location for each individual,

and nearby vertices depend on each other's distance. With these fixed and random effects, a model can be built over which the groups can be statistically compared. This mixed model is as follows:

$$distance_{ij} = \beta_0 + \beta_1 region2_{ij} + \beta_2 region3_{ij} + \beta_3 region4_{ij} + \vartheta_i + \vartheta_j + \epsilon_{ij}$$

In this model, the response variable is the surface distance for the *i*-th individual and the *j*-th vertex is expressed with the following variables:

Fixed Effects:

- β_0 : The intercept, representing the average distance for the reference region (region 1).
- β_1 : The coefficient for region 2, representing the difference in average distance between region 2 and the reference region.
- β_2 : The coefficient for region 3, representing the difference in average distance between region 3 and the reference region.
- β_3 : The coefficient for region 4, representing the difference in average distance between region 4 and the reference region.

Random Effects:

- u_{0i} : The random effect for the *i*-th individual, capturing individual-specific variability.
- v_{0j} : The random effect for the *j*-th vertex, capturing vertex-specific variability.

Residual:

- ϵ_{ij} : The residual error term, representing the unexplained variability in distance for the *i*-th individual and the *j*-th vertex.

For the patella, the mixed model is different compared to the mixed models of the femur and tibia, because the patella is only divided in two regions. RStudio (version 2024.04.01) is used to calculate the results of the mixed model. The results of the mixed models are displayed in Table 2.

Bone	Comparison	Difference in Means	Standard Error	z-Ratio	p-Value
Femur	R1-R2	0.0316	0.0206	1.530	0.4193
	R1-R3	-0.0119	0.0183	-0.649	0.9160
	R1-R4	-0.0587	0.0169	-3.463	0.0030
	R2-R3	-0.0434	0.0185	-2.344	0.0883
	R2-R4	-0.0902	0.0172	-5.251	<0.0001
	R3-R4	-0.0468	0.0143	-3.266	0.0060
Patella	R1-R2	-0.229	0.00879	-26.061	<0.0001
Tibia	R1-R2	0.5965	0.0163	36.505	<0.0001
	R1-R3	-0.5146	0.0174	-29.598	<0.0001
	R1-R4	-0.0699	0.0163	-4.287	0.0001
	R2-R3	-1.1111	0.0171	-65.035	<0.0001
	R2-R4	-0.6664	0.0160	-41.685	<0.0001
	R3-R4	0.4446	0.0171	26.073	<0.0001

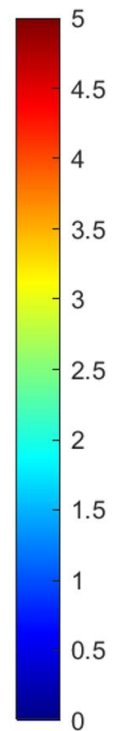
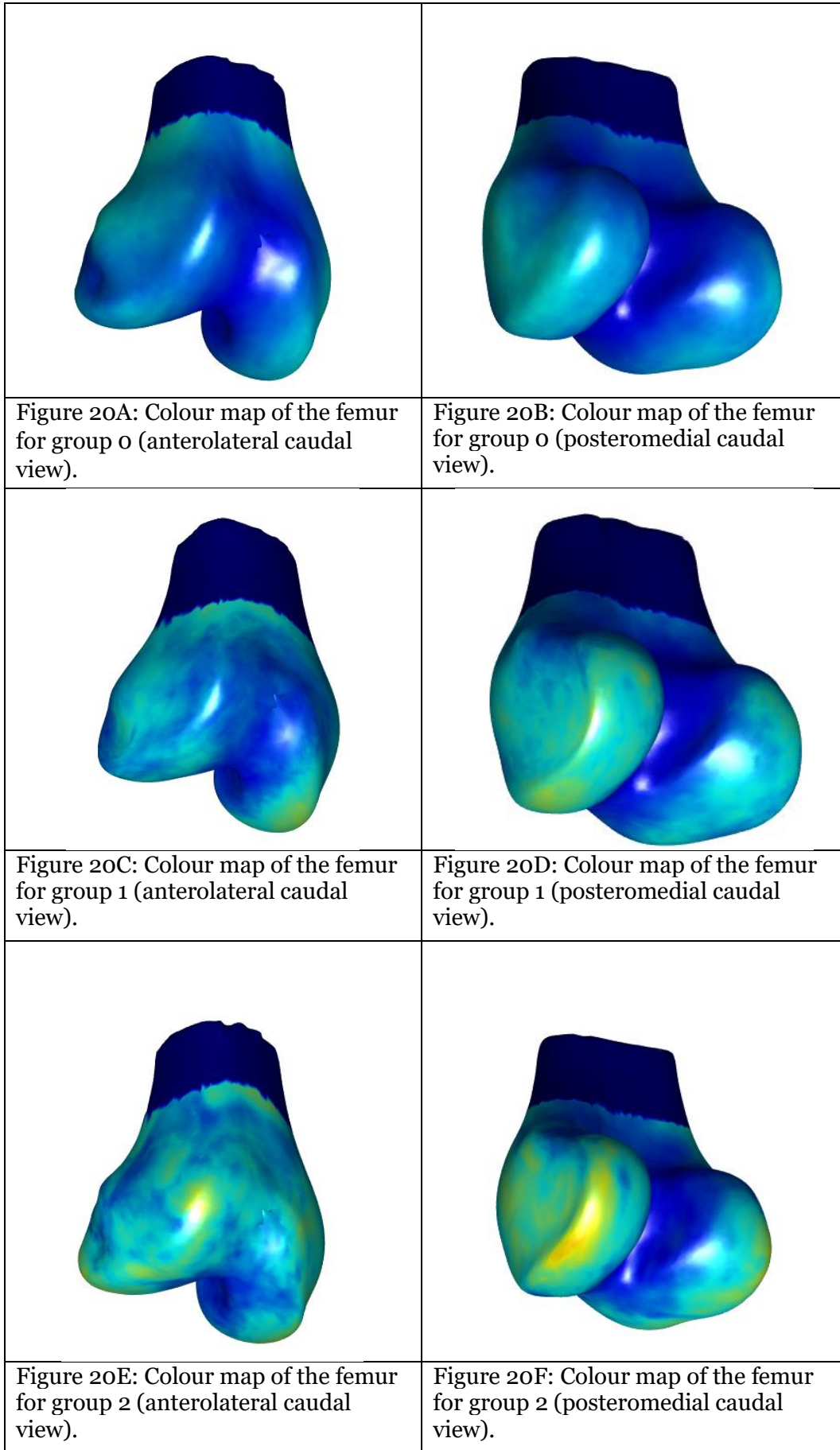
With a confidence level of 0.95, the differences in the regions of the patella and tibia are all significant. The significant difference for the patella indicates that region 2 (medial part of the patella) is more asymmetrical than region 1 (lateral part of the patella). For the tibia, region 2 (medial part of the tibial plateau) exhibits the most bilateral symmetry, whereas region 3 (lateral part of the tibial metaphysis) is the most asymmetrical. For the femur, comparisons involving region 4 (posteromedial part of the femur) are significant, indicating that region 4 is significantly more asymmetrical than the other regions.

7.2 Sub-goal 2

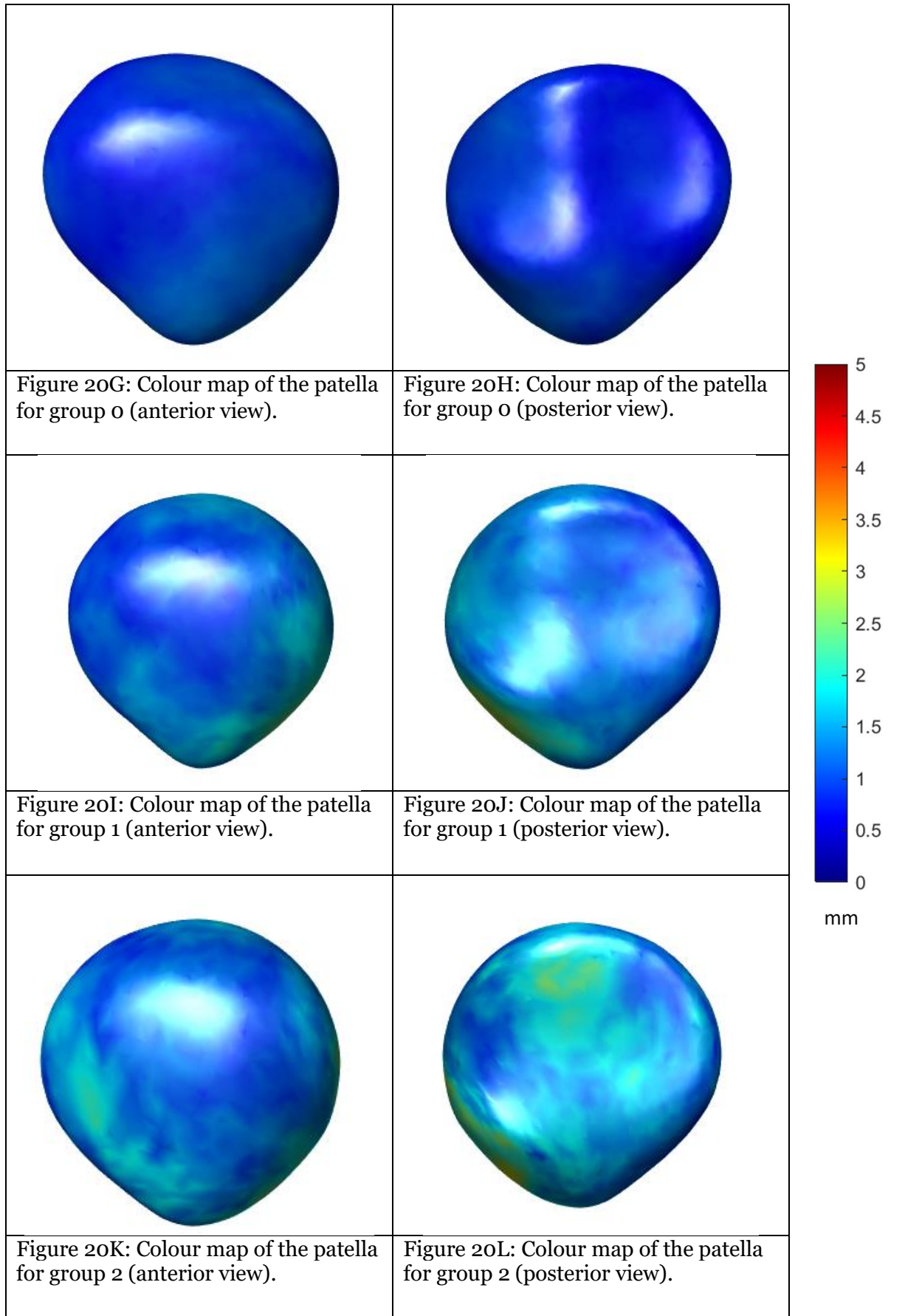
Sub-goal 2 is: 'To examine to which extent and in which regions knees with mild and severe trochlear dysplasia demonstrate greater/less morphological bilateral asymmetry compared to healthy knees.' For this, the groups which contain knees with trochlear dysplasia, groups 1 and 2, are included in the results section. These groups are compared to the group without trochlear dysplasia, group 0.

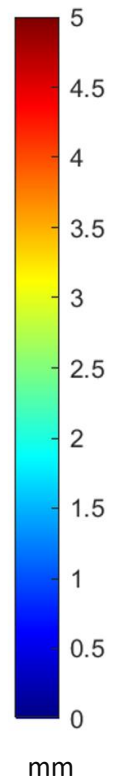
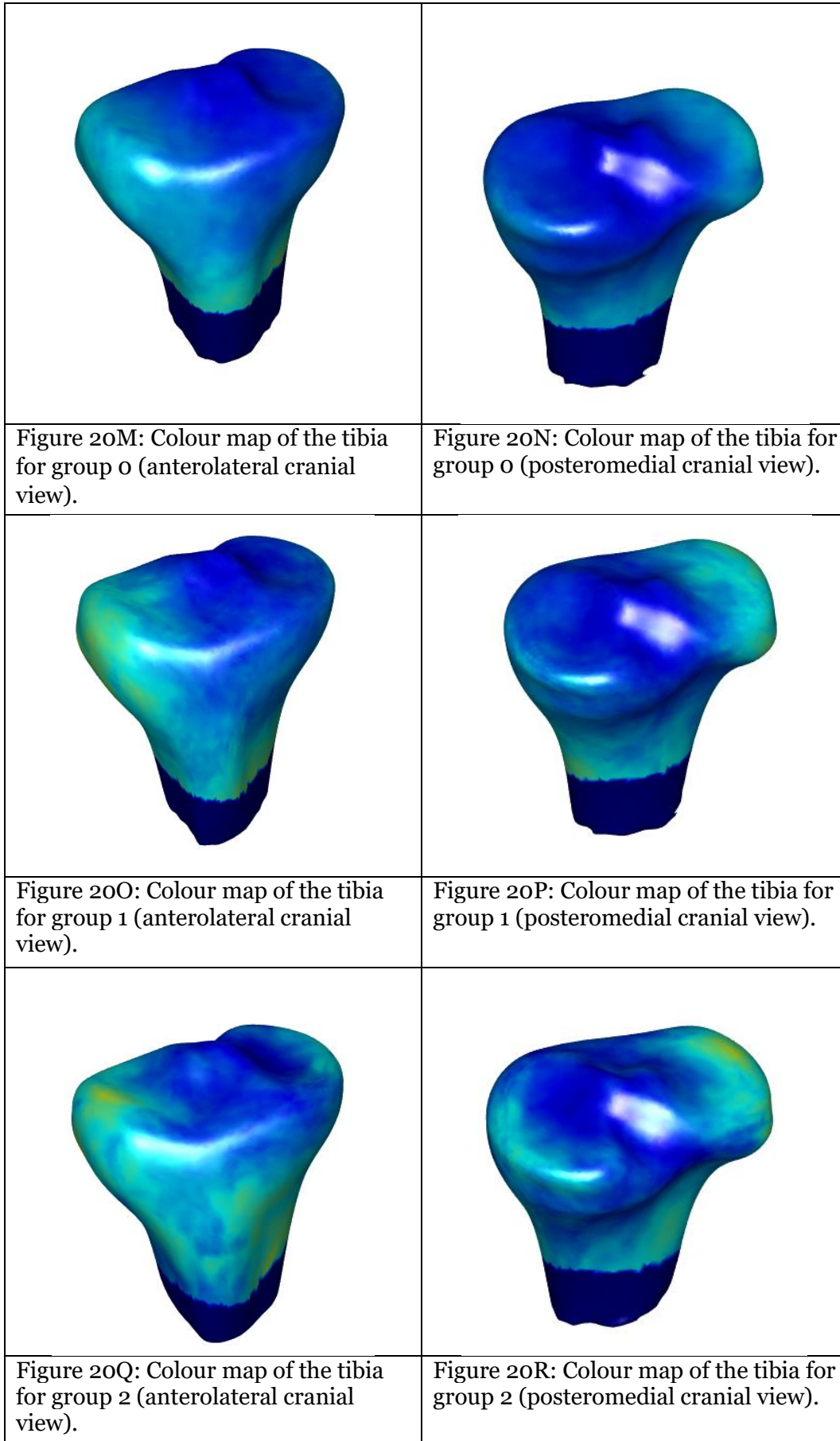
7.2.1 Visualisations

The medians per vertex are shown in the colour maps in Figure 20A-R. In addition to group 0, the colour maps of groups 1 and 2 have now been added so that they can be visually compared.



mm



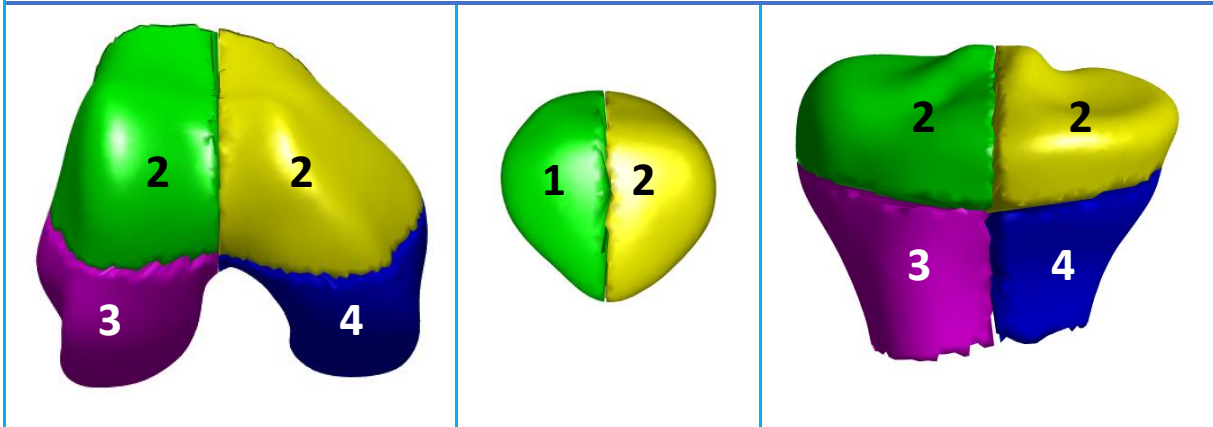


Visually, it is possible to identify differences between groups 0, 1 and 2. In general, there is more highlighting in the colour map in the groups with trochlear dysplasia, with group 2 identifying even more asymmetry than group 1. For the femur, the medial condyle in particular appears to show bilateral asymmetry. For the patella, the medial, caudal surface is more highlighted and the posterior, articular surface also seems to be more asymmetrical than the anterior side. For the tibia, the orange and yellow colours at the lateral part of the tibial plateau are particularly noticeable.

7.2.2 Quantification

Table 3 is similar to the Table 1 in **Section 7.1.2**, but it includes the results for groups 1 and 2, allowing for comparative analysis.

Table 3: Median ± IQR in mm for the femur, patella and tibia, for each group, for the total bone and for the regions.



Bone	Group	Total bone	Region 1	Region 2	Region 3	Region 4
Femur	0 (n=154)	1.3 ± 0.7	0.6 ± 0.1	0.6 ± 0.2	0.5 ± 0.3	0.5 ± 0.3
	1 (n=43)	1.5 ± 0.7	0.8 ± 0.3	0.7 ± 0.2	0.6 ± 0.4	0.6 ± 0.5
	2 (n=18)	1.7 ± 0.9	1.0 ± 0.6	0.9 ± 0.3	0.7 ± 0.5	0.5 ± 0.5
Patella	0 (n=138)	0.9 ± 0.2	0.8 ± 0.2	1.0 ± 0.2		
	1 (n=42)	1.3 ± 0.4	1.1 ± 0.3	1.4 ± 0.4		
	2 (n=18)	1.4 ± 0.5	1.3 ± 0.3	1.5 ± 0.6		
Tibia	0 (n=144)	1.4 ± 0.8	0.7 ± 0.4	0.5 ± 0.2	0.8 ± 0.2	0.7 ± 0.2
	1 (n=43)	1.5 ± 0.9	0.7 ± 0.4	0.5 ± 0.2	0.8 ± 0.2	0.8 ± 0.2
	2 (n=18)	1.5 ± 0.8	0.7 ± 0.4	0.5 ± 0.3	0.8 ± 0.3	0.7 ± 0.3

The results in Table 3 show asymmetries around 1-1.5 mm. When examining these results, the median seems to get higher as the degree of trochlear dysplasia increases. This is particularly the case for the femur and patella.

7.2.3 Statistics

For the second sub-goal, the same statistical method is used as in **Section 7.1.3**, the mixed models method. However, not only are the bone regions compared and tested for asymmetry for this purpose. The groups are also compared among themselves to examine whether there is a difference in morphological bilateral asymmetry. For this comparison, the following model applies.

$$distance_{ij} = \beta_0 + \beta_1 group1_{ij} + \beta_2 group2_{ij} + \vartheta_i + \vartheta_j + \epsilon_{ij}$$

In this model, the response variable is the surface distance for the *i*-th individual and the *j*-th vertex is expressed with the following variables:

Fixed Effects:

- β_0 : The intercept, representing the average distance for the reference group (group 0).
- β_1 : The coefficient for group 1, representing the difference in average distance between region 2 and the reference group.
- β_2 : The coefficient for group 2, representing the difference in average distance between region 3 and the reference group.

Random Effects:

- u_{0i} : The random effect for the *i*-th individual, capturing individual-specific variability.
- v_{0j} : The random effect for the *j*-th vertex, capturing vertex-specific variability.

Residual:

- ϵ_{ij} : The residual error term, representing the unexplained variability in distance for the *i*-th individual and the *j*-th vertex.

This model resulted in the output, displayed by Table 4.

Bone	Comparison	Difference in Means	Standard Error	z-Ratio	p-Value
Femur	G0-G1	-0.5313	0.00268	-198.489	<0.0001
	G0-G2	-0.5997	0.00383	-156.775	<0.0001
	G1-G2	-0.0683	0.00383	-17.865	<0.0001
Patella	G0-G1	-1.068	0.00743	-143.749	<0.0001
	G0-G2	-1.534	0.01051	-145.956	<0.0001
	G1-G2	-0.466	0.01051	-44.310	<0.0001
Tibia	G0-G1	-0.39250	0.00344	-114.087	<0.0001
	G0-G2	-0.40203	0.00492	-81.781	<0.0001
	G1-G2	-0.00953	0.00492	-1.939	0.1277

All comparisons of the groups are significant with a confidence level of 0.95, except for the comparison between group 1 and 2 of the tibia. The results show that the degree of trochlear dysplasia has an effect on the degree of bilateral asymmetry, with more trochlear dysplasia indicating more asymmetry. This effect is thus least present in the tibia, where it is not significant whether there is mild or severe dysplasia.

To test the difference of regions within a bone group, the same model is used as in **Section 7.1.3**, only now groups 1 and 2 have been added. Table 5 describes the results of these mixed models.

Table 5: Results of the mixed models of the regions in the femur, patella and tibia for all three groups.

Bone	Comparison	Difference in Means	Standard Error	z-Ratio	p-Value
Femur Group 0	R1-R2	0.0316	0.0206	1.530	0.4193
	R1-R3	-0.0119	0.0183	-0.649	0.9160
	R1-R4	-0.0587	0.0169	-3.463	0.0030
	R2-R3	-0.0434	0.0185	-2.344	0.0883
	R2-R4	-0.0902	0.0172	-5.251	<0.0001
	R3-R4	-0.0468	0.0143	-3.266	0.0060
Femur Group 1	R1-R2	0.02919	0.0236	1.236	0.6041
	R1-R3	0.03418	0.0210	1.630	0.3618
	R1-R4	0.00577	0.0194	0.297	0.9909
	R2-R3	0.00499	0.0212	0.235	0.9954
	R2-R4	-0.02342	0.0197	-1.190	0.6333
	R3-R4	-0.02841	0.0164	-1.731	0.3074
Femur Group 2	R1-R2	-0.00941	0.0283	-0.332	0.9874
	R1-R3	-0.01235	0.0252	-0.491	0.9611
	R1-R4	0.07594	0.0233	3.261	0.0061
	R2-R3	-0.00294	0.0255	-0.115	0.9994
	R2-R4	0.08535	0.0236	3.614	0.0017
	R3-R4	0.08829	0.0197	4.485	<0.0001
Patella Group 0	R1-R2	-0.229	0.00879	-26.061	<0.0001
Patella Group 1	R1-R2	-0.661	0.0239	-27.699	<0.0001
Patella Group 2	R1-R2	-0.214	0.0306	-6.999	<0.0001
Tibia Group 0	R1-R2	0.5965	0.0163	36.505	<0.0001
	R1-R3	-0.5146	0.0174	-29.598	<0.0001
	R1-R4	-0.0699	0.0163	-4.287	0.0001
	R2-R3	-1.1111	0.0171	-65.035	<0.0001
	R2-R4	-0.6664	0.0160	-41.685	<0.0001
	R3-R4	0.4446	0.0171	26.073	<0.0001
Tibia Group 1	R1-R2	0.0631	0.0202	31.286	<0.0001
	R1-R3	-0.473	0.0214	-22.073	<0.0001
	R1-R4	-0.118	0.0201	-5.862	<0.0001
	R2-R3	-1.104	0.0211	-52.387	<0.0001
	R2-R4	-0.749	0.0197	-37.957	<0.0001
	R3-R4	0.355	0.0210	16.896	<0.0001
Tibia Group 2	R1-R2	0.623	0.0200	31.163	<0.0001
	R1-R3	-0.352	0.0213	-16.561	<0.0001
	R1-R4	0.106	0.0200	5.295	<0.0001
	R2-R3	-0.976	0.0209	-46.659	<0.0001

	R2-R4	-0.518	0.0196	-26.449	<0.0001
	R3-R4	0.458	0.0209	21.947	<0.0001

With a confidence level of 0.95, all regions within all groups of the patella and tibia are significantly different from one another. For the patella, region 2 (medial part of the patella) appears to be more asymmetrical. For the tibia, region 3 (lateral part of the tibial metaphysis) is significantly the most asymmetrical. For the femur, most comparisons are not significant, except for the comparisons of region 4 (posteromedial part of the femur) in group 0 and 2 are significant.

8. Discussion

This study was initiated to investigate the degree of 3D morphological bilateral asymmetry of the bones comprising the knee joint. The aims were to investigate to which extent healthy knees exhibit morphological bilateral symmetry and to examine to which extent and in which regions knees with mild and severe trochlear dysplasia demonstrate greater/less morphological bilateral symmetry compared to healthy knees. The median degree of bilateral asymmetry in healthy knees is 1.3 mm for the femur, 0.9 mm for the patella and 1.4 mm for the tibia. In the healthy knees, several regions are significantly the most asymmetrical, as the posteromedial part of the femur, the medial part of the patella and the lateral part of the tibial metaphysis. This is also the case for the knees with mild and severe trochlear dysplasia. For the three bones, the surface distance increases significantly with a higher degree of dysplasia, but this is more significant for the femur and the patella than for the tibia.

8.1 Comparison with previous research

There is little studied in previous literature regarding morphological bilateral asymmetry at a detailed 3D level as in this study. However, an equivalent study was already conducted for the tibial plateau, which concluded that the tibial plateau had an asymmetry of 0.6 ± 0.03 mm on average for an assessment with 100 sets of healthy knees (25). In this study, the tibial plateau corresponds to regions 1 and 2, which had an asymmetry with a median of 0.7 ± 0.4 mm and 0.5 ± 0.2 mm, respectively. These values are close to the previously conducted study of the tibia plateau. This study, however, mentions the outcome to be clinically neglectable.

Other studies also indicate a certain degree of morphological bilateral asymmetry. For example, studies on the morphological features of the femur and tibia have found several features to be bilaterally asymmetric (56). In a study studying unilateral PFI, it was found that for these cases, the bones of the knees were also not bilaterally equal (47).

8.2 Strengths

There are several strengths of this research. Firstly, we ensured maximum inclusivity in our research. By incorporating a diverse and comprehensive sample set, our findings are more generalisable and reflective of the broader population. This inclusivity strengthens the external validity of our results.

Secondly, the 3D models used in this study were of exceptionally high resolution, featuring a substantial number of vertices. This high level of detail enabled us to perform measurements with a precision of at least 1 mm, ensuring that even the smallest asymmetries could be accurately detected. The ability to measure with such precision is critical in morphological studies where minor variations can be significant.

Additionally, for the categorisation of trochlear dysplasia, we employed the gold standard diagnostic criteria of Dejour. This widely accepted criterion enhances the credibility and diagnostic accuracy of our classifications. Using Dejour as a standard ensures that our findings are aligned with clinical best practices and are widely applicable.

Moreover, the measurements conducted in this study were objective and facilitated by automated algorithms. This approach minimises human error and bias, providing consistent and reproducible results. The use of automated systems also allows for efficient processing of large datasets, which is beneficial in studies with extensive sample sizes.

The methodology demonstrated in this study is versatile, being applicable both on an individual level and across larger groups. The creation of a mean model as a template for group analysis underscores the scalability of our approach, enabling detailed individual assessments while also allowing for comprehensive group comparisons. This dual applicability enhances the utility of our findings for both personalised medicine and broader epidemiological studies.

8.3 Limitations

This study's methodological approach faced several significant issues that could affect the interpretation of our findings. Firstly, it was not entirely known what pathologies the included individuals had. The inclusions were screened for the pathologies registered in the patient record, but this is a limited description and this registration is not always complete. To this end, CT scans of the included knees were examined for possible pathologies that could negatively affect the results of the study. Also, all radiographs (some of which were reconstructed from the CT) were reviewed by an orthopaedic surgeon and the principal investigator, thus rechecking all knees. By examining this, it can be expected that no knees were included with pathologies that would negatively affect the results. However, there is a marginal chance that a set of knees were included that should have been excluded, but we consider this chance to be negligible.

Secondly, due to the unavailability of suitable radiographs for most participants, artificial radiographs were created from CT scans. These artificial images, while assessed, did not replicate clinical images, posing challenges in accurately categorising individuals by degree of trochlear dysplasia. These challenges in categorisation potentially introduce a bias in our evaluation and categorisation process. Besides, it is important to note that a single experienced orthopaedic surgeon performed the categorisation of trochlear dysplasia. While this approach was chosen for consistency and reliability, it raises questions about the reproducibility these results. However, the consistency was evaluated by randomly categorising 11 radiographs twice, whereby 7 out of 11 images were consistently assessed. The double assessment tested the reliability of the categorisation. The score points to moderate reliability, however when looking at another test a better reliability comes out: of the 91 individuals who were known to have patellofemoral complaints were 58 assigned to group 1 or 2. Of the 138 individuals who were not known to have patellofemoral symptoms, 128 classified in group 0. This suggests that individuals with patellofemoral symptoms are possible to be identified by their radiographs, while healthy knees are conveniently distinguishable by their lack of Dejour indicators. Eventually, the categorisation process created three distinct groups, which differ significantly in size. This makes the groups less suitable for comparison.

Additionally, segmentation errors appear to have occurred in some meshes. An example of this is given in Figure 21A and B.



Figure 21A: CT scan with bone fragment.

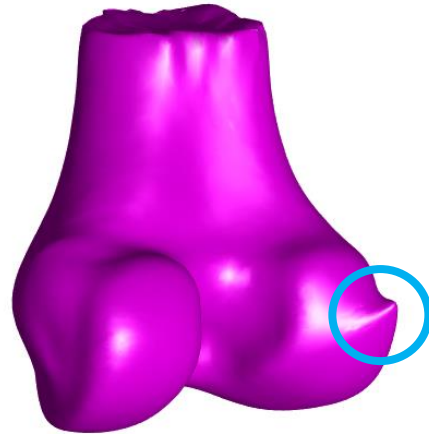


Figure 21B: Resulting segmentation, which is disturbed by the bone fragment.

Here it can be seen that a calcification or loose bone fragment is localised posterior to the femur. In the segmentation, this bone fragment is attached to the femur, creating a protruding part at the femur. This creates an anomalous value when calculating morphological bilateral asymmetry. Another example is the segmentation of this patella, seen in Figure 22A and B. This patella is bipartite, which is usually an asymptomatic finding in 2-3% of people where the patella has not fully merged (57). In about 50% of cases, this development is bilateral. This patella was included in the study, but should have been excluded in view of the resulting segmentations.

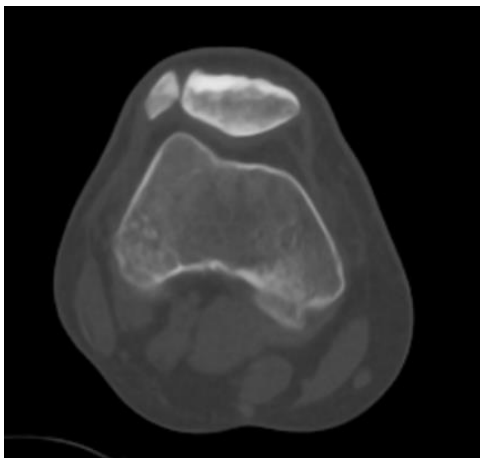


Figure 22A: CT scan with bipartite patella.

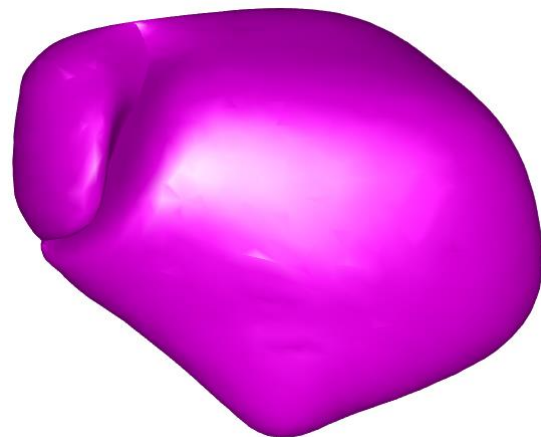


Figure 22B: Resulting segmentation, which is disturbed by the bipartite patella.

Moreover, while processing the data, it was quickly noticed that an artifact appeared around the surface of the mesh where the mesh was cut off in the pre-processing phase of the method. It was decided not to include the 20 mm proximal to the femoral mesh and the distal 20 mm from the tibial mesh when processing the results. Since a cutting plane is not clinically relevant, this decision has a positive influence on the results.

Another limitation is that with the CPD registration that is used to register the mean bones as a template on the various bone components, it is not clear how exactly the points of the template are distributed over the bone component. It is known that the mean bone centralises itself and then morphs towards the points of the surface of the bone component. Because the most central points

are found first during the non-rigid registration, it will be the least sensitive to the deviations (which could be caused by bilateral asymmetry). As a result, the calculation of the surface distances of the central vertices may be underestimated and the calculations of the more external vertices may be overestimated.

Lastly, this study did not focus on the rotational symmetry of the femur, patella and tibia. To determine femoral anteversion, which is a confounding factor for the development of PFI, a measurement that includes the femoral head is important. However, femoral anteversion is correlated with trochlear dysplasia, and would therefore have been interesting to include in this study (58). A follow-up study could be conducted to determine whether femoral anteversion is bilaterally symmetrical and whether this differs between people with and without trochlear dysplasia.

9. Clinical Relevance & Future Perspective

As described in **Chapter 9**, it is important to determine the clinical significance of this study. Since the majority of all data show a bilateral asymmetry of 1-2 mm. The patellofemoral surfaces show the greatest degree of asymmetry. It can also be concluded that the degree of bilateral asymmetry in the femur and patella tends to increase with the severity of trochlear dysplasia. This raises the question whether the degree of asymmetry is such that using the contralateral, asymptomatic side as a surgical reference is justified when performing, for example, a trochleoplasty. If there is a degree of asymmetry between a symptomatic and asymptomatic knee, it can be reasoned that the cause of the complaints may be related to the bony anatomy of the femur and patella.

In this study, it was not possible to determine whether all individuals diagnosed with trochlear dysplasia experienced patellofemoral instability (PFI) symptoms. While the symptom status of some individuals was known, the primary focus was on anatomical abnormalities rather than symptom expression. Future research could investigate the relationship between trochlear dysplasia and the presence of PFI symptoms by examining the degree of morphological bilateral symmetry in patients with unilateral or bilateral instability. This could help determine whether the presentation of uni- or bilateral symptoms has a morphological bony cause.

Additionally, future studies could employ 4DCT scanning to examine uni- and bilateral symptoms at both morphological and kinematic levels. By quantifying and comparing bilateral differences in patients' movements to their morphological differences, researchers could explore whether movement discrepancies are related to bony morphology.

Another clinically relevant finding is that the classification of trochlear dysplasia with the Dejour criteria is complex and prone to errors. In this study, an experienced orthopaedic surgeon assessed the grade of trochlea dysplasia on radiographs and simulated radiographs. In general, assessing knees without dysplasia was considered simple. However, it was not clear on both the clinical and artificial radiographs how the contours of the condyles progressed (and which contour was created by which condyle). This made it confusing whether, for example, a crossing sign could be recognised in a radiograph. The confusing contours raised doubts about assessing some radiographs as 'no dysplasia' and 'severe dysplasia', which could be of significant influence on the results. Thereby, there were individuals who bilaterally received a different Dejour classification during categorisation. These individuals were assigned to the highest group, and thus temporarily considered 'symmetrical' during this study. Looking back at these individuals now, we see that they do not have obviously more bilateral asymmetry than the other individuals: the median of bilateral differences in this group was 2.1 mm. Therefore, an inconsistency exists between the categorisation and the outcome of this methodology. The Dejour criteria are used as golden standard in diagnosing trochlear dysplasia and therefore this was the most suitable method in categorising the groups. Categorising a knee with this method, using a lateral radiograph, is a subjective and inconsistent method. To answer the doubts surrounding the Dejour categorisation, more research could be done into the way in which orthopaedic surgeons use this method to diagnose trochlear dysplasia and whether there is a need for a different categorisation methodology.

Another finding that emerged is the challenge in requesting anonymised radiological data at Radboudumc. Several factors contribute to the complexity of the assessment:

- In this study, the data request took 20 weeks (counting from the day that action was first taken to request data for this study, until the day the last data was sent from the radiology department). This makes the application very time-consuming.

- Having an nWMO number was mandatory when applying, while no nWMO application was required for this study.
- In this study, a request for anonymous data was submitted. In the current protocol of Radboudumc, it was not possible to make an anonymous request, because patient numbers were essential for requesting the data from the radiology department. Because the lists had to be investigated and filtered before submitting to the radiology department, a researcher cannot avoid seeing the patient numbers.
- The selection methods of the data search system are not correct. This is evidenced by the fact that a broad data query was submitted in this study (see **Section 6.2**), which would present all CT scans in ten years from patients between 16 and 40 years old where both knees might be present. This query resulted in 13,444 unique patient numbers, of which 109 scans could be included based on the inclusion and exclusion criteria in Table 1. It is certain that not all scans have been found in the Radboudumc database, because only 17 of the 62 scans of the PFI and PFP group of the already available data were found in the request, where it was expected that all these scans would be found. Due to the failure of the data search system, unnecessary costs were incurred. 601 scans have been invoiced to the orthopaedics department for not-delivered scans, CT scans without knees or other types of imaging.

These obstructions make conducting research at Radboudumc complicated. This could discourage researchers from making a similar data request. This could be improved using a protocol in which the information management and the radiology department would have the same information. The electronic patient dossier search system could be further developed by creating specific labels or keywords, making it possible to search for specific terms within patient files or radiological reports.

10. Conclusion

The morphological bilateral asymmetry of the knee bones measures 1.3 ± 0.7 mm for the femur, 0.9 ± 0.2 mm for the patella, and 1.4 ± 0.8 mm for the tibia. This asymmetry increases notably with the degree of trochlear dysplasia, particularly affecting the femur and patella. The regions with the greatest asymmetry are the medial condyle of the femur (0.5 mm), the medial part of the patella (1.0 mm), and the lateral part of the tibial metaphysis (0.8 mm). Although the bones of the knee exhibit morphological bilateral asymmetry, the degree of asymmetry is generally small and may have limited clinical significance.

11. References

1. Agur AMR, Dalley AFTA-TT. Grant's atlas of anatomy. Fourteenth ed: Wolters Kluwer Philadelphia; 2017.
2. Knee Joint: Cleveland Clinic; 2022 [updated 03/02/2023. Available from: <https://my.clevelandclinic.org/health/body/24777-knee-joint>.
3. Yamada Y, Toritsuka Y, Yoshikawa H, Sugamoto K, Horibe S, Shino K. Morphological analysis of the femoral trochlea in patients with recurrent dislocation of the patella using three-dimensional computer models. *J Bone Joint Surg Br.* 2007;89(6):746-51.
4. Wang C, Li T-J, Zheng Y-P. Shear Modulus Estimation on Vastus Intermedius of Elderly and Young Females over the Entire Range of Isometric Contraction. *PloS one.* 2014;9:e101769.
5. Stewardship RD. CliniQuestCore: Radboudumc; 2023 [Available from: <https://www.experiencept.rehab/blog/quadriceps>.
6. Vaienti E, Scita G, Ceccarelli F, Pogliacomì F. Understanding the human knee and its relationship to total knee replacement. *Acta Biomed.* 2017;88(2s):6-16.
7. Koh JL, Stewart C. Patellar instability. *Orthop Clin North Am.* 2015;46(1):147-57.
8. Nita C. Medial Patellofemoral Ligament (MPFL) Reconstruction [12-10-2023]. Available from: <https://www.northernkneeclinic.co.uk/surgical-procedures/medial-patellofemoral-ligament-mpfl-reconstruction/>.
9. Moore KL, Agur AMR, Dalley AF. *Essential Clinical Anatomy*: Lippincott Williams & Wilkins; 2011.
10. Loes Schiphouwer SvdG, Margreet van Olst, Albert van Kampen. *Patellofemorale instabiliteit*. 2015.
11. David Dejour SZ, Elizabeth A. Arendt, Petri Sillanpää, Florian Dirisamer. *Patellofemoral Pain, Instability, and Arthritis*: Springer Berlin, Heidelberg; 2020. 582 p.
12. *Patellar Dislocation and Instability: OrthoManhattan*; [Available from: <https://adamcohenmd.com/patellar-instability>].
13. Parikh SN, Lykissas MG, Gkiatas I. Predicting Risk of Recurrent Patellar Dislocation. *Curr Rev Musculoskelet Med.* 2018;11(2):253-60.
14. Wildt Jd. *Spieren van de heup: Kniecare*; 2020 [Available from: <https://kniecare.nl/kennisbank/spieren-van-de-heup/>].
15. Saccomanno MF, Maggini E, Vaisitti N, Pianelli A, Grava G, Cattaneo S, Milano G. Sulcus Angle, Trochlear Depth, and Dejour's Classification Can Be Reliably Applied To Evaluate Trochlear Dysplasia: A Systematic Review of Radiological Measurements. *Arthroscopy.* 2023;39(2):549-68.
16. Kazley JM, Banerjee S. Classifications in Brief: The Dejour Classification of Trochlear Dysplasia. *Clin Orthop Relat Res.* 2019;477(10):2380-6.
17. Dean C, Chahla J, Serra Cruz R, Cram T, LaPrade R. Patellofemoral Joint Reconstruction for Patellar Instability: Medial Patellofemoral Ligament Reconstruction, Trochleoplasty, and Tibial Tubercle Osteotomy. *Arthroscopy Techniques.* 2016;5.
18. Caton J, Deschamps G, Chambat P, Lerat JL, Dejour H. [Patella infera. Apropos of 128 cases]. *Rev Chir Orthop Reparatrice Appar Mot.* 1982;68(5):317-25.
19. Ntagiopoulos P, Bonin N, Sonnery-Cottet B, Badet R, Dejour D. The incidence of trochlear dysplasia in anterior cruciate ligament tears. *International orthopaedics.* 2014;38.
20. Hysing-Dahl T, Inderhaug E, Faleide AGH, Magnussen LH. Patients' experiences of living with patellar instability before and after surgery: a qualitative interview study. *BMJ Open.* 2023;13(6):e072141.
21. Zhang YQ, Zhang Z, Wu M, Zhou YD, Tao SL, Yang YL, et al. Medial patellofemoral ligament reconstruction: A review. *Medicine (Baltimore).* 2022;101(1):e28511.

22. Reagan J, Kullar R, Burks R. MPFL reconstruction: technique and results. *Orthop Clin North Am.* 2015;46(1):159-69.
23. Nita C. Medial Patellofemoral Ligament (MPFL) Reconstruction 2023 [Available from: <https://www.northernkneeclinic.co.uk/surgical-procedures/medial-patellofemoral-ligament-mpfl-reconstruction/>].
24. Song EK, Seon JK, Kim MC, Seol YJ, Lee SH. Radiologic Measurement of Tibial Tuberosity-Trochlear Groove (TT-TG) Distance by Lower Extremity Rotational Profile Computed Tomography in Koreans. *Clin Orthop Surg.* 2016;8(1):45-8.
25. Dunning H. The knee in motion. Dynamic CT imaging for diagnosis and evaluation of knee disorders: Radboud University; 2023.
26. Harvey CJ. Principles of radiology. Surgery (Oxford). 2008;26(6):235-8.
27. Tanaka MJ, Sodhi A, Wadhavkar I, Kane K, Velasquez Hammerle MV, Mangudi Varadarajan K, Tornetta P. Redefining Trochlear Dysplasia: Normal Thresholds Vary by Measurement Technique, Landmarks, and Sex. *The American Journal of Sports Medicine.* 2023;51(5):1202-10.
28. Stepanovich M, Bomar JD, Pennock AT. Are the Current Classifications and Radiographic Measurements for Trochlear Dysplasia Appropriate in the Skeletally Immature Patient? *Orthop J Sports Med.* 2016;4(10):2325967116669490.
29. The Knee under Rotation [Internet]. 2018 [cited 2-4-2024].
30. Wang J, Fleischmann D. Improving Spatial Resolution at CT: Development, Benefits, and Pitfalls. *Radiology.* 2018;289:181156.
31. Lee WG. Principles of CT: Radiation Dose and Image Quality. *Journal of Nuclear Medicine Technology.* 2007;35(4):213.
32. Raman SP, Mahesh M, Blasko RV, Fishman EK. CT Scan Parameters and Radiation Dose: Practical Advice for Radiologists. *Journal of the American College of Radiology.* 2013;10(11):840-6.
33. Selles M, van Osch JAC, Maas M, Boomsma MF, Wellenberg RHH. Advances in metal artifact reduction in CT images: A review of traditional and novel metal artifact reduction techniques. *European Journal of Radiology.* 2024;170:111276.
34. Wong MT, Wiens C, Kuczynski M, Manske S, Schneider PS. Four-dimensional computed tomography: musculoskeletal applications. *Can J Surg.* 2022;65(3):E388-e93.
35. Tryggestad E, Li H, Rong Y. 4DCT is long overdue for improvement. *Journal of Applied Clinical Medical Physics.* 2023;24(4):e13933.
36. Kwong Y, Mel AO, Wheeler G, Troupis JM. Four-dimensional computed tomography (4DCT): A review of the current status and applications. *J Med Imaging Radiat Oncol.* 2015;59(5):545-54.
37. Ambellan F, Lamecker H, von Tyrowicz C, Zachow S. Statistical Shape Models: Understanding and Mastering Variation in Anatomy. *Adv Exp Med Biol.* 2019;1156:67-84.
38. Patil A, Kulkarni K, Xie S, Bull AMJ, Jones GG. The accuracy of statistical shape models in predicting bone shape: A systematic review. *Int J Med Robot.* 2023;19(3):e2503.
39. Jolliffe IT, Cadima J. Principal component analysis: a review and recent developments. *Philosophical Transactions of the Royal Society A: Mathematical, Physical and Engineering Sciences.* 2016;374(2065):20150202.
40. Joshua Cates SE, Ross Whitaker. *Statistical Shape and Deformation Analysis*: Elsevier; 2017.
41. Yamada Y, Toritsuka Y, Horibe S, Nakamura N, Sugamoto K, Yoshikawa H, Shino K. Patellar instability can be classified into four types based on patellar movement with knee flexion: a three-dimensional computer model analysis. 2018. p. 328-35.
42. Leclerc JT, Dartus J, Labreuche J, Martinot P, Galmiche R, Migaud H, et al. Complications and outcomes of trochleoplasty for patellofemoral instability: A systematic review and meta-analysis of 1000 trochleoplasties. *Orthop Traumatol Surg Res.* 2021;107(7):103035.
43. Peng HM, Feng B, Chen X, Wang YO, Bian YY, Wang W, et al. Usefulness of a Simple Preoperative Planning Technique using Plain X-rays for Direct Anterior Approach for Total Hip Arthroplasty. *Orthop Surg.* 2021;13(1):145-52.

44. Ten Berg PW, Dobbe JG, van Wolfswinkel G, Strackee SD, Streekstra GJ. Validation of the contralateral side as reference for selecting radial head implant sizes. *Surg Radiol Anat.* 2016;38(7):801-7.
45. Maderbacher G, Keshmiri A, Zeman F, Grifka J, Baier C. Assessing joint line positions by means of the contralateral knee: a new approach for planning knee revision surgery? *Knee Surg Sports Traumatol Arthrosc.* 2015;23(11):3244-50.
46. van der Gaast N, Dunning H, Huitema JM, Waters A, Jaarsma RL, Doornberg JN, et al. The symmetry of the left and right tibial plateau: a comparison of 200 tibial plateaus. *European Journal of Trauma and Emergency Surgery.* 2023;49(1):69-74.
47. Chen J, Huang X, Xu Z, Zhang H, Zhou A, Zhao P, Yin L. Ipsilateral patellofemoral morphological abnormalities are more severe than those of contralateral joints in patients with unilateral patellar dislocation. *Knee Surg Sports Traumatol Arthrosc.* 2021;29(8):2709-16.
48. Lowekamp B, Chen D, Ibanez L, Blezek D. The Design of SimpleITK. *Frontiers in Neuroinformatics.* 2013;7.
49. Isensee F, Jaeger PF, Kohl SAA, Petersen J, Maier-Hein KH. nnU-Net: a self-configuring method for deep learning-based biomedical image segmentation. *Nature Methods.* 2021;18(2):203-11.
50. Nacey NC, Fox MG, Luce BN, Boatman DM, Diduch DR. Assessing Femoral Trochlear Morphologic Features on Cross-Sectional Imaging Before Trochleoplasty: Dejour Classification Versus Quantitative Measurement. *American Journal of Roentgenology.* 2020;215(2):458-64.
51. Jacob S, Mahalingam H. Medial condyle hypoplasia in adolescent and young adult patients with trochlear dysplasia: a retrospective study. *Radiol Bras.* 2023;56(6):321-6.
52. Keshmiri A, Schöttle P, Peter C. Trochlear dysplasia relates to medial femoral condyle hypoplasia: an MRI-based study. *Arch Orthop Trauma Surg.* 2020;140(2):155-60.
53. Qiu L, Li J, Sheng B, Yang H, Xiao Z, Lv F, Lv F. Patellar shape is associated with femoral trochlear morphology in individuals with mature skeletal development. *BMC Musculoskelet Disord.* 2022;23(1):56.
54. Dai Y, Li H, Li F, Lin W, Wang F. Association of Femoral Trochlear Dysplasia and Tibiofemoral Joint Morphology in Adolescent. *Med Sci Monit.* 2019;25:1780-7.
55. Frosch S, Brodkorb T, Schüttrumpf JP, Wachowski MM, Walde TA, Stürmer KM, Balcarek P. Characteristics of femorotibial joint geometry in the trochlear dysplastic femur. *J Anat.* 2014;225(3):367-73.
56. Eckhoff DG, Jacofsky DJ, Springer BD, Dunbar M, Cherian JJ, Elmallah RK, et al. Bilateral Symmetrical Comparison of Femoral and Tibial Anatomic Features. *The Journal of Arthroplasty.* 2016;31(5):1083-90.
57. Atesok K, Doral NM, Lowe J, Finsterbush A. Symptomatic Bipartite Patella: Treatment Alternatives. *JAAOS - Journal of the American Academy of Orthopaedic Surgeons.* 2008;16(8):455-61.
58. Liebensteiner MC, Ressler J, Seitlinger G, Djurdjevic T, El Attal R, Ferlic PW. High Femoral Anteversion Is Related to Femoral Trochlea Dysplasia. *Arthroscopy.* 2016;32(11):2295-9.

Appendix

For aspects of this research, it was decided not to include this in the general chapters of the research, such as the codes used to generate the results, the settings used to create the mean models and the results per included individual. The following appendix sections contain this relevant additional information from the study.

A. MATLAB Codes

The MATLAB scripts referenced throughout the methodology detailed in **Chapter 6** played a pivotal role in executing various procedural steps. This section aims to provide an overview of each script within the research workflow.

A1. Creating the Bone Meshes

This code contains components that create meshes from the masks, saved as an MHA file. The meshes are set to 20,000 faces, which usually results in a number of vertices of ~10,000. The meshes are saved so that they can be used in other steps.

```

side = {'left', 'right'};

% Loop through CT folders
for i = 1:100
    % Generate the folder name
    folderName = sprintf('CT_%04d', i);
    % Construct the full path to the folder
    folderPath = fullfile(baseFolder, folderName);

    % Check if the folder exists
    if exist(folderPath, 'dir')
        % Construct the file path to the .mha file
        filePath = fullfile(folderPath, 'mask', 'T_0.mha');
        % Check if the .mha file exists
        if exist(filePath, 'file')
            % Read the .mha file and calculate 'stat' variable
            try
                for sd = 1:2
                    [stat.(side{sd}).fem, stat.(side{sd}).pat, stat.(side{sd}).tib,
~] = mhamask2mesh(filePath, side{sd}, '123', 20000, 2);

                    fem.(side{sd}).V = stat.(side{sd}).fem.vertices;
                    fem.(side{sd}).F = stat.(side{sd}).fem.faces;

                    pat.(side{sd}).V = stat.(side{sd}).pat.vertices;
                    pat.(side{sd}).F = stat.(side{sd}).pat.faces;

                    tib.(side{sd}).V = stat.(side{sd}).tib.vertices;
                    tib.(side{sd}).F = stat.(side{sd}).tib.faces;

                    [sCS.(side{sd}), ~, ~] = ERCKneeReferenceFrames(fem.(side{sd}),
pat.(side{sd}), tib.(side{sd}));
                end
                % Construct the full file name to save 'stat'
                statFileName = fullfile(folderPath, 'stat_sCS.mat');
                % Save 'stat' and sCS variables
                save(statFileName, 'stat', 'sCS');

                % Store the file path in the cell array
                filePaths{end+1} = filePath;
            catch
            end
        end
    end
end

```

```

        catch exception
            fprintf('Error processing folder %s: %s\n', folderName,
exception.message);
        end
    end
end
end
end

```

A2. Mirror the Bone Meshes

In this code the left meshes are mirrored over the x-axis. This aligns all bones as 'right' bones in the following steps. By mirroring, the bones can be compared.

```

% left
for i = 1:numWorkspaces

    if isempty(femurs(i).V)
        continue; % Skip to the next iteration if the cell is empty
    end

    femurs_m(i).V = femurs(i).V*(eye(3).*[-1 1 1]);
    femurs_m(i).F = femurs(i).F;
end

% right
for i = numWorkspaces+1:2*numWorkspaces

    if isempty(femurs(i).V)
        continue; % Skip to the next iteration if the cell is empty
    end

    femurs_m(i).V = femurs(i).V;
    femurs_m(i).F = femurs(i).F;
end

```

A3. Cut the Bone Meshes

The bone meshes of the femur and tibia are cut off in the method. In the following code this is applied to femoral meshes. The widest point of the bone is taken and used to cut the height of the bone with this distance. This allows the bones to be better proportionally registered in a later step in the method.

```

for i = 1:numWorkspaces

    if isempty(femurs_m(i).V)
        continue; % Skip to the next iteration if the cell is empty
    end

    % The distance in mm to make the cut
    cutDist = (max(femurs_m(i).V(:,1))-min(femurs_m(i).V(:,1)));

    extremity = max(femurs_m(i).V(:,3), [], 'all');
    distpoint = extremity + cutDist;
    cPlane_one = plane2iplane([0 0 distpoint 0 0 1]);

    % Cut
    [facesCut{i}, verticesCut{i},~,~] =
cutMeshWithPlane2(femurs_m(i).F, femurs_m(i).V, cPlane_one, 1, -1);
end

```

A4. CPD Registration

CPD registration is applied twice in the registration of the bones. The first time, the mean bone is rigidly reregistered on the bone component. In the calculation, the position of the mean bone is already translated to the position of the left and right bone components, to prevent large translations. In the second registration, the rigidly registered mean bone is non-rigidly registered on the left and right bone components, so that the points of the mean bone take over the surface of these bone components. This step contributes to the calculation of the surface distances between the left and right bone components in a later step.

```

verticesR2 = cell(1,numBones);

verticesR3 = cell(1,numBones);

verticesL2 = cell(1,numBones);

verticesL3 = cell(1,numBones);

% left
for i = 1:numBones
    if isempty(verticesL{i})
        continue; % Skip to the next iteration if the cell is empty
    end
    optBone.method = 'rigid';
    optBone.normalize = true; % Normalise to unit variance and zero mean
    optBone.corresp = 1:length(verticesL{1,i}); % Correspondence indices for femur
    optBone.outliers=0.3;

    % CPD registration
    [registered1, ~] = cpd_register(verticesL{i},vertices0-
mean(vertices0)+mean(verticesL{i}), optBone);
    verticesL2{i} = registered1.Y;
    close

    % Initialise CPD parameters
    optBone.method = 'nonrigid';
    optBone.normalize = true; % Normalise to unit variance and zero mean
    optBone.corresp = 1:length(vertices0); % Correspondence indices for femur
    optBone.lambda = 0.5;
    optBone.beta = 1.5;
    optBone.tol= 1e-5;
    optBone.outliers=0.01;

    [registered2, ~] = cpd_register(verticesL{i}, verticesL2{i}, optBone);
    verticesL3{i} = registered2.Y;
    close
    disp(sprintf('This was left iteration %d.', i))
end

% right
for i = 1:numBones
    if isempty(verticesR{i})
        continue; % Skip to the next iteration if the cell is empty
    end
    optBone.method = 'rigid';
    optBone.normalize = true; % Normalise to unit variance and zero mean
    optBone.corresp = 1:length(vertices0); % Correspondence indices for femur
    optBone.outliers=0.3;

```

```

% CPD registration R
[registered1, ~] = cpd_register(verticesR{i}, vertices0-
mean(vertices0)+mean(verticesR{i}), optBone);
verticesR2{i} = registered1.Y;
close
% Initialise CPD parameters
optBone.method = 'nonrigid';
optBone.normalize = true; % Normalise to unit variance and zero mean
optBone.corresp = 1:length(vertices0); % Correspondence indices for femur
optBone.lambda = 0.5;
optBone.beta = 1.5;
optBone.tol= 1e-5;
optBone.outliers=0.01;

[registered2, ~] = cpd_register(verticesR{1,i}, verticesR2{i}, optBone);
verticesR3{i} = registered2.Y;
close
disp(sprintf('This was right iteration %d.', i))

end

```

A5. Calculate Distances and Create the Colour maps

The bilateral symmetry is expressed in differences in surface distances. These are calculated by determining the absolute distance between the rigidly registered mean bone and the non-rigidly registered mean bone for both left and right. The differences between the calculations of left and right are seen as the surface distances between left and right, and thus express a degree of symmetry. Because a distance is calculated for each point in the mesh, this can be linked to a colour code in a colour map. The mean bone can be visualised, with a colour that expresses the bilateral distances. For the femur and tibia, a specific region was selected, which did not use the upper and lower 20 mm of the bone in the calculation, respectively, due to the cutting artifact.

```

% right
for i = 1:numel(verticesR2)
distancesR{1,i} = abs(verticesR2{1,i}-verticesR3{1,i});
end

% left
for i = 1:numel(verticesL2)
distancesL{1,i} = abs(verticesL2{1,i}-verticesL3{1,i});
end

% distance between R and L
for i = 1:numel(distancesR)
distancesRL{1,i} = abs(distancesR{1,i}-distancesL{1,i});
end

cat_dist = cat(3,distancesRL{:});
median_dist = median(cat_dist,3);

for i = 1:length(median_dist)
distance(i,1) = norm(median_dist(i,:));
end

median_distance = median(distance(region_indices));
distance(setdiff(1:size(vertices0, 1), region_indices), :) = 0;
distances = distance(region_indices);

```

A6. Create an Artificial Radiography

The following code was used to create artificial radiographs, in the case where no suitable clinical radiography was available. It is important to mention that the radiography calculations are done using the code 'GetLateralRadiographs' available from the orthopaedic research lab data. In short, rotations are calculated in that code that provide a lateral display. A Python code is called that rotates the images with the results of those calculations. A ROI is then selected around the patella. The intensity of a fluoroscopy is calculated per pixel in the radiography and the radiography is finished.

```
% Define side and bone names
side = {'left', 'right'};

% Specify the output folder
outputBaseFolder = 'C:\...';

% Loop through patient folders
for pt = 1:100
    % Generate the folder name
    folderName = sprintf('CT_%04d', pt);
    % Construct the full path to the patient folder
    patientFolder = fullfile(baseFolder_CT, folderName);

    % Check if the stat_sCS.mat file exists in the patient folder
    statFile = fullfile(patientFolder, 'stat_sCS.mat');
    if exist(statFile, 'file')
        try
            % Load stat and sCS variables from the stat_sCS.mat file
            load(statFile, 'stat', 'sCS');

            % Construct the full path to the mha folder
            mhaFolder = fullfile(patientFolder, 'mha');
            % Check if the mha folder exists
            if ~exist(mhaFolder, 'dir')
                error('MHA folder not found in folder %s', folderName);
            end

            % Load mha file
            mhaFile = fullfile(mhaFolder, 'T_0.mha');
            if exist(mhaFile, 'file')
                % Loop through sides (left and right)
                for sd = 1:2
                    % Set side name
                    sde = side{sd};

                    % Define output folder for this side
                    outputFolder = fullfile(outputBaseFolder, folderName, sde);
                    % Make sure the output folder exists
                    if ~exist(outputFolder, 'dir')
                        mkdir(outputFolder);
                    end

                    % Call GetLateralRadiographs function
                    [imprjrot.(side{sd})] = GetLateralRadiographs(patientFolder,
outputFolder, stat, sCS, sde);
                    end

                    % Save the output variable imprjrot
                    save(fullfile(outputBaseFolder, folderName, 'imprjrot.mat'),
'imprjrot');
                else
                    error('MHA file not found in folder %s', mhaFolder);
                end
            catch exception
                fprintf('Error processing folder %s: %s\n', folderName,
exception.message);
            end
        end
    end
end
```

```

        end
    else
        fprintf('stat_sCS.mat file not found in folder %s\n', folderName);
    end
end
end

```

B. ShapeWorks Settings

Table 6 shows the settings which are used in the ShapeWorks software to create the mean models. The settings are based on the default settings and optimised based on the tips provided by the software publisher. The optimisation was necessary to distribute the particles over the entire surfaces.

Number of Particles	1000 (patella: 500)
Initial Relative Weighting	1
Relative Weighting	1
Starting Regularization	1000
Ending Regularization	10
Iterations per Split	1000
Optimization Iterations	1000
Procrustes	√
Procrustes Scaling	√
Procrustes Rotation/Translation	√
Procrustes Interval	10
Narrow Band	1